

ORIGINAL ARTICLE

Perivascular localized cells commit erythropoiesis in PDGF-B-expressing solid tumors

Kayoko Hosaka¹ | Chenchen Wang^{2,3} | Shiyue Zhang^{2,3} | Xue Lv^{2,3} | Takahiro Seki¹ | Yin Zhang^{1,4} | Xu Jing^{1,5} | Jieyu Wu¹ | Qiqiao Du¹ | Xingkang He^{1,6} | Yulong Fan^{2,3} | Xuan Li^{2,3} | Makoto Kondo⁷ | Masahito Yoshihara⁸  | Hong Qian⁷ | Lihong Shi^{2,3} | Ping Zhu^{2,3} | Yuanfu Xu^{2,3} | Yunlong Yang⁹  | Tao Cheng^{2,3} | Yihai Cao¹ 

¹Department of Microbiology, Tumor and Cell Biology, Karolinska Institute, Stockholm, Sweden

²State Key Laboratory of Experimental Hematology, National Clinical Research Center for Blood Diseases, Haihe Laboratory of Cell Ecosystem, Institute of Hematology & Blood Diseases Hospital, Chinese Academy of Medical Sciences & Peking Union Medical College, Tianjin, P. R. China

³Tianjin Institutes of Health Science, Tianjin, P. R. China

⁴School of Pharmacology, Binzhou Medical University, Yantai, Shandong, P.R. China

⁵Department of Clinical Laboratory, the Second Hospital of Shandong University, Jinan, Shandong, P. R. China

⁶Department of Gastroenterology, Sir Run Run Shaw Hospital, Zhejiang University Medical School, Hangzhou, Zhejiang, P.R. China

⁷Center for Hematology and Regenerative Medicine, Department of Medicine, Karolinska Institute, Karolinska University Hospital, Stockholm, Sweden

⁸Department of Biosciences and Nutrition, Karolinska Institute, Huddinge, Sweden

⁹Department of Cellular and Genetic Medicine, School of Basic Medical Sciences, Fudan University, Shanghai, P. R. China

Correspondence

Yihai Cao, Department of Microbiology, Tumor and Cell Biology, Karolinska Institute, Stockholm 17177, Sweden.
 Email: yihai.cao@ki.se

Tao Cheng, State Key Laboratory of Experimental Hematology, National Clinical Research Center for Blood

Abstract

Background: Tumors possess incessant growth features, and expansion of their masses demands sufficient oxygen supply by red blood cells (RBCs). In adult mammals, the bone marrow (BM) is the main organ regulating hematopoiesis with dedicated manners. Other than BM, extramedullary hematopoiesis is discovered in various pathophysiological settings. However, whether tumors can

List of abbreviations: APC, allophycocyanin; BFU-E, burst-forming unit-erythroid; BM, bone marrow; CAF, cancer-associated fibroblast; CD31, cluster of differentiation 31; CD34, cluster of differentiation 34; CD71, cluster of differentiation 71; DAF, 2,7-diaminofluorene; EGFP, enhancing green fluorescent protein; ELISA, enzyme-linked immunosorbent assay; EPO, erythropoietin; FACS, fluorescence-activated cell sorting; FBS, fetal bovine serum; GO, gene ontology; GSEA, gene set enrichment analysis; HPC, hematopoietic progenitor cell; HSPC, hematopoietic stem and progenitor cell; LLC, Lewis lung cancer; MEP, megakaryocyte-erythroid progenitors; MSCV, murine stem cell virus; NG2, neural/glial antigen 2; PBS, phosphate-buffered saline; PCA, principal component analysis; PDGF, platelet-derived growth factor; PDGFR, platelet-derived growth factor receptor; qPCR, quantitative polymerase chain reaction; RBC, red blood cell; SCA1, stem cell antigen-1; SCID, severe combined immunodeficiency; TME, tumor microenvironment; TSO, template switch oligo; UMAP, uniform manifold approximation and projection.

Kayoko Hosaka, Chenchen Wang, Shiyue Zhang and Xue Lv contributed equally to this work.

This is an open access article under the terms of the [Creative Commons Attribution-NonCommercial-NoDerivs](https://creativecommons.org/licenses/by-nc-nd/4.0/) License, which permits use and distribution in any medium, provided the original work is properly cited, the use is non-commercial and no modifications or adaptations are made.

© 2023 The Authors. *Cancer Communications* published by John Wiley & Sons Australia, Ltd. on behalf of Sun Yat-sen University Cancer Center.

Diseases, Haihe Laboratory of Cell Ecosystem, Institute of Hematology & Blood Diseases Hospital, Chinese Academy of Medical Sciences & Peking Union Medical College, Tianjin 300020; Tianjin Institutes of Health Science, Tianjin 301600, P. R. China.
Email: chengtao@ihcams.ac.cn

Funding information

CAMS Innovation Fund for Medical Sciences, Grant/Award Number: 2021-I2M-1-017; National Natural Science Foundation of China, Grant/Award Number: 81970107; State Key Laboratory of Experimental Hematology Research, Grant/Award Number: Z22-02; Tianjin “131” Science Fund for Creative Research Groups, Grant/Award Number: 2021; Swedish Research Council, Grant/Award Numbers: 2016-02215, 2019-01502, 2020-06121, 2021-06122; National Key R&D Program of China, Grant/Award Number: 2020YFC0846600; Hong Kong Centre for Cerebro-cardiovascular Health Engineering; Swedish Cancer Foundation, Grant/Award Number: 200734PjF; Swedish Children’s Cancer Foundation, Grant/Award Number: PR2018-0107; Strategic Research Areas (SFO)-Stem Cell and Regenerative Medicine Foundation; Karolinska Institute distinguished professor award; Karolinska Institute Foundation; Scandinavia-Japan Sasakawa Foundation, Grant/Award Number: 81801163; Doctor Fund of Shandong Natural Science Foundation, Grant/Award Number: ZR201807060846; Japan Society for the Promotion of Science (JSPS) Overseas Research Fellowships

contribute to hematopoiesis is completely unknown. Accumulating evidence shows that, in the tumor microenvironment (TME), perivascular localized cells retain progenitor cell properties and can differentiate into other cells. Here, we sought to better understand whether and how perivascular localized pericytes in tumors manipulate hematopoiesis.

Methods: To test if vascular cells can differentiate into RBCs, genome-wide expression profiling was performed using mouse-derived pericytes. Genetic tracing of perivascular localized cells employing *NG2-CreERT2:R26R-tdTomato* mouse strain was used to validate the findings in vivo. Fluorescence-activated cell sorting (FACS), single-cell sequencing, and colony formation assays were applied for biological studies. The production of erythroid differentiation-specific cytokine, erythropoietin (EPO), in TME was checked using quantitative polymerase chain reaction (qPCR), enzyme-linked immunosorbent assay (ELISA, magnetic-activated cell sorting and immunohistochemistry. To investigate BM function in tumor erythropoiesis, BM transplantation mouse models were employed.

Results: Genome-wide expression profiling showed that in response to platelet-derived growth factor subunit B (PDGF-B), neural/glial antigen 2 (NG2)⁺ perivascular localized cells exhibited hematopoietic stem and progenitor-like features and underwent differentiation towards the erythroid lineage. PDGF-B simultaneously targeted cancer-associated fibroblasts to produce high levels of EPO, a crucial hormone that necessitates erythropoiesis. FACS analysis using genetic tracing of NG2⁺ cells in tumors defined the perivascular localized cell-derived subpopulation of hematopoietic cells. Single-cell sequencing and colony formation assays validated the fact that, upon PDGF-B stimulation, NG2⁺ cells isolated from tumors acted as erythroblast progenitor cells, which were distinctive from the canonical BM hematopoietic stem cells.

Conclusions: Our data provide a new concept of hematopoiesis within tumor tissues and novel mechanistic insights into perivascular localized cell-derived erythroid cells within TME. Targeting tumor hematopoiesis is a novel therapeutic concept for treating various cancers that may have profound impacts on cancer therapy.

KEYWORDS

cancer, hematopoiesis, PDGF-B, perivascular localized cell, stem cell, tumor vasculature

1 | BACKGROUND

Solid tumors emblemize a multicellular machinery constructed by malignant cells and various stromal cells, such as cancer-associated fibroblasts (CAFs), tumor-associated macrophages, vascular endothelial cells, perivascular cells, immune cells, adipocytes, and even stem cells [1–4]. The cancerous machinery exhibits several distinct features, including: (1) infinite growth and expansion of malignant cells [1]; (2) switching to an angiogenic phenotype

[5]; (3) high-grade of inflammation [6, 7]; (4) recruitment and activation of CAFs [8, 9]; (5) suppression of immune cell functions [10, 11]; (6) experiencing high levels of tissue hypoxia [12]; (7) high expression of various growth factors and cytokines [13]; (8) spreading to distal tissues and organs [14, 15]; (9) heterogeneity of various cellular populations [16, 17]; (10) alteration of metabolism [18, 19]; and (11) insensitive responses to drugs [20, 21]. Because of these unique features, development of effective therapeutic modalities becomes a challenging and

unmanageable issue for most cancer types in human patients.

Owing to relentless genetic mutations and instability, heterogeneous and mosaic cancer cell populations exist in tumor tissue and the ratio of these mosaic populations alters along with cancer progression [1]. Solid tumors contain a high density of micro-vasculatures that are created by endothelial cells and perivascular cells [22–25]. Vascular endothelial cells and perivascular cells are abundant cellular components in the tumor microenvironment (TME) and display multiple functions, including angiogenesis, vascular permeability, vascular remodeling, vascular survival, vascular-tumor paracrine communications, recruiting other stromal cells, such as monocytes/macrophages and immune cells, and providing progenitor cells [26]. Heterogeneity of malignant cells and various stromal cellular components determine the diverse expression of different growth factors and cytokines. Platelet-derived growth factors (PDGFs) are commonly expressed in tumors and target stromal fibroblasts and perivascular cells through binding to platelet-derived growth factor receptors (PDGFRs) including PDGFR α or PDGFR β [23, 27–29]. While angiogenic endothelial cell-derived PDGFs promote the recruitment of pericytes onto newly formed vessels [30–32], high levels of tumor cell-derived PDGFs can ablate pericytes from tumor vasculatures [33–35].

In adult mammals, erythropoiesis in physiological conditions mainly occurs in the bone marrow (BM) through a tightly regulated mechanism of hematopoietic progenitor differentiation [23, 36–40]. Hierarchy mechanisms that underlie committing differentiation of hematopoietic stem cells (HSCs) towards different lineages are regulated with great precision by various growth factors and cytokines [41–46]. For example, erythropoietin (EPO) is essential for myeloid progenitor cells to become erythroblasts [47, 48]. Under physiological conditions, EPO production is primarily restricted to the kidney and it regulates erythropoiesis through binding to EPO receptor (EpoR) expressed in erythroblast progenitor cells [47, 48]. During embryogenesis and certain pathological conditions, extramedullary hematopoiesis, i.e., hematopoiesis outside of the BM, occurs in other tissues and organs, including the yolk sac, liver, and spleen [49, 50]. Hematopoiesis may also occur in the lungs, a process called pulmonary hematopoiesis, by producing platelets from megakaryocytes [51].

Albeit various organs and tissues were found to process extramedullary hematopoiesis under certain pathophysiological settings, whether solid tumors, which show incessant growth features and demands for sufficient oxygen supply by red blood cells (RBCs), can contribute to hematopoiesis is completely unknown. Accumulating evidence shows that, pericytes retain progenitor cell properties and can differentiate into various cell types, including

adipocytes, chondrocytes, osteoblasts, phagocytes, granulocytes, muscle, and fibroblasts [33, 52–54]. The PDGF-B signaling is well known for regulating pericyte functions including recruitment into and coverage of micro-vessels. Under physiological conditions, endothelial cells are the primary source of PDGF-B [24]. In this investigation, we sought to better understand under pathological conditions, such as a PDGF-B-rich TME, whether and how perivascular localized pericytes manipulate hematopoiesis.

2 | MATERIALS AND METHODS

2.1 | Animals

All animal studies were approved by the North Stockholm Animal Ethical Committee in Sweden (Stockholm, Sweden) or the Institutional Animal Care and Use Committee at the Institute of Hematology, Chinese Academy of Medical Sciences (Tianjin, P.R. China). Euthanasia protocols and their humane endpoints are adhered to by ethical permits. Six- to eight-week-old C57BL/6, severe combined immune deficient (SCID), and *neural/glial antigen 2 (NG2)-CreERT2:R26R-tdTomato* mice were obtained from the animal facility in the Department of Microbiology, Tumor and Cell Biology, Karolinska Institute, Stockholm, Sweden. For tumor experiments, *NG2-CreERT2:R26R-tdTomato* mice were orally treated every other day in total five times with 100 mg/kg of tamoxifen. Tumor tissues were harvested 5–7 days after the last treatment. Six- to 8-week-old C57BL/6-Ly5.2 (Ly5.2, CD45.2) and C57BL/6-Ly5.1 (Ly5.1, CD45.1) mice were bred and maintained in the animal facility of the Institute of Hematology, Chinese Academy of Medical Sciences. The cages were maintained under a 12-h dark/12-h light cycle with food and water provided ad libitum. All animals that met the provisions of the Animal Ethics participated in the study.

2.2 | Cell culture and transfection

Mouse Lewis lung carcinoma cell line (LLC) and mouse fibrosarcoma cell line (T241) were purchased from the American Type Culture Collection (ATCC; Manassas, Virginia, USA). Human epidermoid carcinoma cell line (A431) was kindly provided by Dr. Keiko Funa, Gothenburg University, Sweden. All cell lines were grown and maintained in a Dulbecco's modified Eagle's medium (DMEM, SH30243.01, HyClone, Logan, UT, USA) supplemented with 10% fetal bovine serum (FBS; SH30160.03, HyClone), 100 U/mL penicillin, and 100 μ g/mL streptomycin (SV30010, HyClone) at 37°C with 5% CO₂. All cell lines were routinely tested for mycoplasma

contaminations by Mycoplasma detection kit (LT07-318, Lonza, Basel, Switzerland) to ensure negative results.

PDGF-B- or vector-transfected LLC and T241 cells were established by an eGFP⁺ murine stem cell virus (MSCV) vector (provided by Dr. Robert Pawliuk at Massachusetts Institute of Technology). Briefly, for transfection, complementary deoxyribonucleic acids (cDNAs) containing human platelet-derived growth factor-B (*PDGFB*) were cloned into the MSCV vector including enhanced green fluorescent protein (EGFP). Retroviral supernatants were generated by transfecting retroviral constructs into human embryonic kidney 293 cells with the large T antigen of simian virus 40 (HEK293T) with expression plasmids encoding ecotropic gag/pol and the vesicular stomatitis virus-glycoprotein (VSV-G) envelope using a calcium orthophosphate (CaPO₄) transfection method. Mouse tumor cell lines grown in a culture plate were incubated with filtered viral supernatants for 6 h and cultured for two consecutive days. GFP-positive cells were sorted using a FACStar+ (Becton Dickinson, San Jose, CA, USA) and amplified cells were further used for experiments.

shPDGFB-A431 cells were established using a lentiviral vector-based expression packaging kit (GeneCopoeia, Rockville, Maryland, USA) by a specific shRNA targeting *PDGFB* mRNA. The transfection method was followed according to the manufacturer's protocol. Briefly, to produce *PDGFB* shRNA viral particles, *PDGFB* shRNA containing plasmid and viral packaging vectors were co-transfected into HEK293T cells. Viral particles, including *PDGFB* shRNA, were collected from the conditioned medium and were subsequently used to infect A431 cells. The transduced cells were selected using puromycin (A11138-02, Invitrogen, Waltham, MA, USA) in a culture medium.

2.3 | Xenograft tumor models

Approximately $1-2 \times 10^6$ murine LLC and T241 tumor cells in 0.1 mL Phosphate-buffered saline (PBS) were subcutaneously injected into the middle region of the dorsal back with one location or the abdominal side with two locations in each mouse. For human tumor study, approximately 5×10^6 A431 tumor cells in 0.1 mL PBS were subcutaneously injected into the abdominal side at two locations in each SCID mouse. Tumor volume was calculated using the formula ($\text{length} \times \text{width}^2 \times 0.52$), and tumor tissues were harvested when the tumor size reached around 0.8-1.2 cm³. In some cases, tumor-bearing mice were intraperitoneally treated with a rat anti-mouse PDGFR α neutralizing antibody (IH3, 40 mg/kg, twice per week, ImClone Pharmaceuticals, kindly provided by Dr. Zhenping Zhu) or a rat anti-mouse PDGFR β neutralizing antibody (2C5,

40 mg/kg, twice per week, ImClone Pharmaceuticals, kindly provided by Dr. Zhenping Zhu), an anti-mouse EPO-specific neutralizing antibody (200 $\mu\text{g}/\text{kg}$; three times per week, AF959, R&D SYSTEM), and recombinant human EPO (2000 IU/kg; three times per week). Mice were sacrificed by a lethal dosage of CO₂ or inhalation of high dosage isoflurane followed by cervical dislocation.

2.4 | BM transplantation

Six- to 8-week-old C57BL/6-Ly5.2 (Ly5.2, CD45.2) recipient mice were exposed twice to a dose of 4.5 Gy by X-ray with a 4h interval. After 24 h, BM cells were collected from C57BL/6-Ly5.1 (Ly5.1, CD45.1) donor mice. After removing RBCs by an RBC lysis buffer (MA0207, Meilunbio, China), approximately 1×10^7 whole BM cells were intravenously transplanted into each of the recipient mice. Multilineage repopulation of donor myeloid and lymphoid cells was assessed monthly by staining the peripheral blood with antibodies against CD45.1 (1:100, 110741, Biolegend, San Diego, CA, USA) and CD45.2 (1:100, 552950, BD Biosciences, San Jose, CA, USA). After 8-weeks of BM transplantation, mice were used for further experiments.

2.5 | Fluorescence-activated cell sorting (FACS)

For tumor sample preparation, fresh tumor tissues were cut into small pieces and incubated at 37°C with 0.15% collagenase I (17100-017, Gibco, Waltham, MA, USA) and 0.15% collagenase II (17101015, Gibco) in PBS for 30-40 min. Cell suspensions were filtrated with a cell filter with 70- μm -diameter holes, followed by centrifugation at 1500 rpm for 5 min. Single-cell suspensions were subjected to flow cytometry. BM cells were isolated by flushing out from the mouse femur bone. Single-cell suspensions from various samples were incubated with primary antibodies at 4°C for the indicated time points. After primary antibody staining, cells were washed with PBS, followed by flow cytometry, or stained with a secondary antibody at 4°C for 30 min. Antibodies against Fc Receptors (1:10, 130-092-575, Miltenyi Biotec, Bergisch Gladbach, Germany) were applied for FACS. The antibodies and reagent used in our experiments: a PE/Cyanine7-conjugated anti-mouse Ly-6A/E (Sca-1) antibody (1:100, 108114, Biolegend, San Diego, CA, USA), an APC-conjugated anti-mouse CD117 (c-Kit) antibody (1:100, 105812, Biolegend), a rabbit anti-mouse NG2 antibody (1:100, AB5320, Millipore, Burlington, MA, USA), a Brilliant Violet 510-conjugated anti-mouse CD45.1 antibody (1:100, 110741, Biolegend), a PerCP-Cy5.5-conjugated anti-mouse CD45.2 antibody (1:100, 552950,

BD Biosciences, San Jose, CA, USA), a PE/Cyanine7-conjugated anti-mouse B220 antibody (1:100, 103222, Biolegend), a Brilliant Violet 605-conjugated anti-mouse CD45 Antibody (1:100, 103139, Biolegend), a PE-conjugated anti-mouse Ter119 antibody (1:100, 116208, Biolegend), a Brilliant Violet 421-conjugated anti-mouse/human CD11b antibody (1:100, 101236, Biolegend), an APC-conjugated anti-mouse CD71 antibody (1:100, 113820, Biolegend; 1:100, 17-0711-81, eBioscience, San Diego, CA, USA), an APC-conjugated anti-mouse Ter119 antibody (1:100, 17-5921-81, eBioscience), an APC/Cyanine7-conjugated anti-mouse Ter119 antibody (1:100, 116223, Biolegend), a Pacific Blue-conjugated anti-mouse Ly-6A/E (Sca-1) antibody (1:100, 108120, Biolegend), an APC/Cyanine7-conjugated anti-mouse CD117 (c-Kit) antibody (1:100, 105826, Biolegend), and an Alexa Fluor 568-conjugated goat anti-rabbit IgG H&L secondary antibody (1:2000, ab175471, Abcam, Cambridge, UK), 4',6-diamidino-2-phenylindole (DAPI) (1:3000, 422801, Biolegend). The APC-eFluor780-conjugated anti-mouse Lin⁻ cocktail included: an APC-eFluor780-conjugated anti-mouse CD3e antibody (1:100, 47-0031-82, eBioscience), an APC-eFluor780-conjugated anti-mouse CD4 antibody (1:100, 47-0041-82, eBioscience), an APC-eFluor780-conjugated anti-mouse CD8a antibody (1:100, 47-0081-82, eBioscience), an APC-eFluor780-conjugated anti-mouse CD11b antibody (1:100, 47-0112-82, eBioscience), an APC-eFluor780-conjugated anti-mouse Gr-1 antibody (1:100, 47-5931-82, eBioscience), an APC-eFluor780-conjugated anti-human/mouse CD45R(B220) antibody (1:100, 47-0452-82, eBioscience), and an APC-eFluor780-conjugated anti-mouse Ter119 antibody (1:100, 47-5921-82, eBioscience). The PE/Cyanine5-conjugated anti-mouse Lin⁻ cocktail includes a PE/Cyanine5-conjugated anti-mouse CD3e antibody (1:100, 100310, Biolegend), a PE/Cyanine5-conjugated anti-mouse NK1.1 antibody (1:100, 108716, Biolegend), a PE/Cyanine-conjugated anti-mouse Gr-1 antibody (1:100, 108410, Biolegend), a PE/Cyanine5-conjugated anti-human/mouse CD19 antibody (1:100, 15-0193-83, eBioscience), and a PE/Cyanine5-conjugated anti-mouse Ter119 antibody (1:100, 116210, Biolegend). Dead cells were excluded by 7AAD for multi-color staining. Lin⁻Sca-1⁺c-Kit⁺ (LSK) hematopoietic stem and progenitor (HSPC) and the more differentiated progenitor (HPC, Lin⁻Sca-1⁻c-Kit⁺) were gated according to fluorescence minus one (FMO) in samples from *NG2 Cre ERT2:R26R-tdTomato* tumor-bearing mice. LSK and Lin⁻Sca-1⁺ populations using C57BL/6 mice samples were gated according to the BM LSK gate setting. The cell subsets were sorted or analyzed on FACS Aria III (BD, Franklin Lakes, NJ, USA), FACS Canto II (BD), and FACSCalibur (BD). Data were analyzed using FlowJo software (TreeStar Inc., San Francisco, CA, USA) or a

CellQuest software (BD). Gating strategies are presented in corresponding [supplementary figures](#).

2.6 | Magnetic-activated cell sorting

Tissue samples of PDGF-B- or vector-transfected LLC and T241 tumors were cut into small pieces and incubated with 1.5 mg/mL type I (17018029, Gibco) and 1.5 mg/mL II collagenase (17101015, Gibco) in PBS at 37°C for 40-60 min. After filtering with a cell filter, cells were centrifuged at 1500 rpm for 10 min. Cell pellets were collected and incubated with a rabbit anti-mouse NG2 antibody (1:50, AB5320, Millipore), a rat anti-mouse CD31 antibody (1:50, 553370, BD Pharmingen, San Diego, CA, USA), a rat anti-mouse PDGFR α antibody (1:50, 14-1401-82, eBioscience), a rat anti-mouse PDGFR β antibody (1:50, 14-14012-82, eBioscience), and a rat anti-F4/80 antibody (1:200, NBP2-12506, Novus Biologicals, Littleton, CO, USA), followed by species matched antibody incubation in ice, including a Cy5-labeled goat anti-rabbit antibody (1:200, AP132S; Millipore) or Cy5-labeled goat anti-rat antibody (1:200, AP183, Millipore) for 30 min. Cells were further washed and incubated with anti-Cy5/Alexa Fluor 647-coated microbeads (130-091-395, Miltenyi Biotec) for 15 min, and subsequently subjected to magnetic separation through magnetic columns. Collected positive cells were used for further study or stored in RNAlater (R0901, Sigma-Aldrich, Burlington, MA, USA) at -70°C until further use.

2.7 | Hematopoietic colony formation assay

Lin⁻/Sca1⁺/NG2⁺ (L⁻S⁺NG2⁺) cells or NG2⁺ cells isolated from tumor tissues in methylcellulose-based medium were used for single-cell colony formation assay. L⁻S⁺NG2⁺ cells were directly sorted into 48-well plates containing 500 μ L M3434 medium (03434, Stemcell Technologies, Vancouver, Canada). After 14 days, colonies were counted and photographed. Cultured cells were collected for further analyses by gene expression or FACS. NG2⁺ cells isolated using a magnetic-activated cell sorting system were cultured in an M3334 medium (03334, Stemcell Technologies) for 3 days. Colonies were counted and photographed. In some experiments, NG2⁺ cells were treated with 100 ng/mL PDGF-B (315-18, PeproTech, Rocky Hill, New Jersey, USA), 100 ng/mL PDGF-A (315-17, PeproTech), and 100 ng/mL PDGF-D recombinant proteins (1159-SB, R&D SYSTEM), a rat anti-mouse PDGFR α neutralizing antibody (100 μ g/mL, IH3, ImClone Pharmaceuticals, kindly provided by Dr. Zhenping Zhu), and a rat anti-mouse PDGFR β neutralizing antibody (100 μ g/mL,

2C5, ImClone Pharmaceuticals, kindly provided by Dr. Zhenping Zhu). These proteins or antibodies were added into the medium in the assay. In combination with PDGF-B, a rat anti-mouse PDGFR α neutralizing antibody or a rat anti-mouse PDGFR β neutralizing antibody was added 1 h prior to PDGF-B treatment. For single-cell colony formation assay using a liquidized culture medium system, isolated L⁻S⁺NG2⁺ cells were used for further colony characterization analysis. Liquidized culture medium contained α -MEM (C12571500BT, Gibco), 10% FBS (10099-141, Gibco), 1% penicillin/streptomycin (15140122, Gibco), 10 ng/mL IL-3 (213-13, PeproTech, Rocky Hill, NJ, USA), 50 ng/mL SCF (250-03, PeproTech), 50 ng mL⁻¹ TPO (315-14, PeproTech), and 1 U/mL EPO (S19980074, 3SBio Inc, Shenyang, China). After 14-day culture, cells were fixed and stained with a Giemsa staining solution (EMD Chemicals, Gibbstown, NJ, USA). The number of colonies with > 50 cells was scored. BM cells were used in parallel as a positive control.

2.8 | Hemoglobin staining

A mixture of 0.03 g/mL 4,4'-Diaminobiphenyl (Benzidine base, B-3503, Sigma, Missouri, USA) solution, 10% acetic acid (33209, Sigma), and 30% H₂O₂ solution (H1009, Sigma), or a mixture of a freshly prepared 10 mg/mL 2,7-Diaminofluorene (DAF, D17106, Sigma) solution, 30% H₂O₂, and 200 mmol/L Tris HCl (pH 7.5) buffer was used to stain colonies. Positive signals were captured using light microscopy (Nikon Eclipse TS100, Nikon, Tokyo, Japan) equipped with a camera (DS-Fi1, Nikon) and software (NIS-Elements F3.0).

2.9 | Giemsa staining

L⁻S⁺NG2⁺-derived colonies were placed on a slide after being resuspended in 2% FBS/Iscove's modified Dulbecco's Medium (IMDM). After sequential incubation with methanol, Giemsa (32884, Sigma), and Giemsa buffer (pH 6.4; 1.11373, Sigma-Aldrich) for 20 min at room temperature, slides were then washed with distilled water. After staining, air-dried cells were observed under light microscopy and photographed (SMZ18, Nikon). Cells were classified into different stages of erythroblast. BM-derived cell colonies were used as a positive control.

2.10 | Enzyme-linked immunosorbent assay (ELISA)

PDGF-B- or vector-transfected LLC and T241 tumor tissues, and shPDGFB-A431 and shCont-A431 tumor tissues

were homogenized in a protein lysis buffer (C3228, Merck, New Jersey, USA) containing 1% proteinase inhibitor (P8340, Merck), followed by centrifugation at 10,000 rpm for 20 min. Supernatants were collected and stored at -70°C until further use. The mEPO ELISA (MEP00B, R&D Systems) was used to detect mouse EPO levels by the manufacturer protocol.

2.11 | Immunohistochemistry

Frozen tissue samples from PDGF-B- and vector-transfected LLC tumors and shPDGFB-A431 and shCont-A431 tumors were embedded in the OCT compound (4583, Sakura Finetek, CA, USA) and sectioned using a cryostat, followed by fixation with 4% paraformaldehyde (PFA; 441244, Sigma-Aldrich) for 30 min. Tumor tissue slides were stained with a rabbit anti-mouse EPO antibody (1:300; orb6017, Biorbyt, Cambridge, UK), and co-stained with a rat anti-mouse PDGFR α antibody (1:300; 14-1401-82, eBioscience) and a rat anti-mouse PDGFR β antibody (1:300; 14-14012-82, eBioscience), followed by incubation with species-matched secondary antibodies, including an Alexa Fluor 488-labeled goat anti-rat antibody (1:400; A11006, Invitrogen) and an Alexa Fluor 555-labeled goat anti-rabbit antibody (1:400; A21482, Invitrogen). Tumor tissues were counterstained with DAPI. Positive signals were detected using a fluorescence microscope equipped with a camera (DS-Qi1MC, Nikon) and analyzed by a software (NIS-Element F3.0, Nikon). Randomized images were analyzed using an Adobe Photoshop software (CS5; Adobe, San Jose, CA, USA) program.

2.12 | Whole-mount staining

Tumor tissues grown in NG2-CreERT2:R26R-tdTomato mice were collected and fixed overnight with 4% PFA. Thin-sliced tumor tissues were digested for 5 min with 20 mmol/L proteinase K (EO0491, Thermo Fisher Scientific, Waltham, MA, USA) in 10 mmol/L Tris buffer (pH 7.4), followed by incubation with 100% methanol for 30 min. Digested tissues were washed twice in PBS and incubated overnight with 3% skim milk (3187, Semper, Stockholm, Sweden) and 0.3% Triton X-100 (Sigma-Aldrich) in PBS. Samples were further incubated with a rabbit anti-mouse NG2 (1:200; AB5320, Millipore), a rabbit anti-mouse c-KIT antibody (1:200; MAB1356, R&D Systems), a rat anti-mouse CD34 antibody (1:200; ab8158, Abcam), a rat anti-mouse Sca-1 antibody (1:200; MAB1226, R&D Systems), a rat anti-mouse Ter119 antibody (1:200; 55065, BD Pharmingen), and a rat anti-mouse CD71 antibody (1:200; 553264, BD Pharmingen). Species-matched secondary antibodies were

used, including; an Alexa Fluor 647-labeled goat anti-rat (1:200; A21247, Invitrogen) and a Cy5-labelled goat anti-rabbit (1:200; AD132S, Millipore). After rigorous washing, samples were mounted using a Vectashield mounting medium (Vector Laboratories, Burlingame, CA, USA) and signals were analyzed using confocal microscopy (Nikon C1 Confocal microscope, Nikon) equipped with C1 software. Positive signals were analyzed using an Adobe Photoshop software (CS5; Adobe) program.

2.13 | Quantitative polymerase chain reaction (qPCR)

RNAs were extracted from various tumor tissues, isolated cell populations, and cultured cells using TRIzol (79306, Qiagen, Venlo, Netherlands) or a 2-mercaptoethanol-containing lysis buffer (C3228, Millipore), followed by purification using GeneJET RNA Purification Kits (K7032, Thermo Fisher Scientific). Total RNAs were measured with a NanoDrop 2000C Spectrophotometer (Thermo Fisher Scientific), and cDNAs were synthesized using a RevertAid cDNA synthesis kit (K1632, Thermo Fisher Scientific). cDNA samples were subjected to qPCR using SYBER Green (4367659, Applied Biosystems, Waltham, MA, USA) in a StepOnePlus system (Applied Biosystems). Data were presented as relative quantification. The specific primers used in this study included: *Gata1* forward, 5′-CCCCAGTCTTTCAGGTGTATCC-3′; *Gata1* reverse, 5′-GGTGAGCCCCAGGAATT-3′; *Klf1* forward, 5′-AGACTGTCTTACCCTCCATCAG-3′; *Klf1* reverse, 5′-GGTCCTCCGATTTTCAGACTCAC-3′; *Alas2* forward, 5′-GCAGGGCAACAGGACTTTG-3′; *Alas2* reverse, 5′-ACAGGACCGTAGCAACATAGC-3′; *Hba* forward, 5′-CACCACCAAGACCTACTTCC-3′; *Hba* reverse, 5′-CAGTGGCTCAGGAGCTTGA-3′; *Hbb* forward, 5′-TTTAACGATGGCCTGAATCACTT-3′; *Hbb* reverse, 5′-CAGCACAATCACGATCATATTGC-3′; *Hba-x* forward, 5′-GGATCCGGTCAACTTCAAGCT-3′; *Hba-x* reverse, 5′-CGTGCGGCCATTGTGA-3′; *Hbb-y* forward, 5′-CTTGCTCTGCTTCTGCCATA-3′; *Hbb-y* reverse, 5′-CCTTCTTGCCATGGGCTTT-3′; *Hbb-bh1* forward, 5′-GGGAAACCCCGGATTAGA-3′; *Hbb-bh1* reverse, 5′-CCCCAAGCCCAAGGATGT-3′; *Hbb-bh2* forward, 5′-GAGTGAGCTGCACCATGACAA-3′; *Hbb-bh2* reverse, 5′-CATGCTGCCAGGAGCTT-3′; *Gar1* forward, 5′-CAAGGGCCTCCAGAACGTG-3′; *Gar1* reverse, 5′-AAACAGGGCGTTGAAGTAGG-3′; *Epor* forward, 5′-GGGCTCCGAAGAAGTCTGTG-3′; *Epor* reverse, 5′-ATGACTTTCGTGACTCACCT-3′; *Actin* forward, 5′-AGGCCAGAGCAAGAGAGG-3′; *Actin* reverse, 5′-TACATGGCTGGGGTGTGAA-3′; *Epo* forward, 5′-AGAATGGAGGTGGAAGAACAGG-3′; *Epo*

reverse, 5′-CTGGTGGCTGGGAGGAATT-3′; *Pdgfra* forward, 5′-TGCCATGATGCTCGATTCTA-3′; *Pdgfra* reverse, 5′-CGCTGAGGTGGTAGAAGGAG-3′; *Pdgfrb* forward, 5′-TTCAGAGGCAGGAAGGTGCT-3′; *Pdgfrb* reverse, 5′-TCAACGACTCACCAGTGCTC-3′; *Cspg4* forward, 5′-GCTGTCTGTTGACGGAGTGTT-3′; *Cspg4* reverse, 5′-CGGCTGATTCCCTTCAGGTAAG-3′; *Car1* forward, 5′-GACTGGGGATATGGAAGCGAA-3′; *Car1* reverse, 5′-TGCAGGATTATAGGAGATGCTGA-3′; *Actin* forward, 5′-AGGCCAGAGCAAGAGAGG-3′; *Actin* reverse, 5′-TACATGGCTGGGGTGTGAA-3′; *EPO* forward, 5′-AGCCGAGTCCTGGAGAGG-3′; *EPO* reverse, 5′-CTGGAGGGGAATGGCTTCC-3′; *GAPDH* forward, 5′-CATTTCTGGTATGACAACGA-3′; *GAPDH* reverse, 5′-GTCTACATGGCAACTGTGAG-3′.

2.14 | Single-cell RNA sequencing (RNA-seq) library preparation

Single-cell RNA-seq using FACS-isolated L⁻S⁺ NG2⁺ cells from tumor tissue cell fraction was conducted according to the modified Smart-seq2 protocol as previously described [55, 56]. After cDNA amplification, 94 single cells with different barcodes were pooled for one library. The mixed cDNAs were purified by a DNA Clean and Concentration Kit (D4014, ZYMO, California, USA), followed by removing the small fragments and primers (<200 bp) by 0.8 × AMPure XP beads (A63882, Beckman, California, USA). The 30~40 ng purified products were performed with 4 cycles of PCR to append the biotin index to the 3′ end of PCR products. The purified PCR products were fragmented into ~300-bp using Covaris S220 (Covaris). Dynabeads MyOne Streptavidin C1 (65001, Invitrogen) was used for the biotin enrichment of shared cDNAs. The library was constructed using KAPA Hyper Prep Kits (KK8504, Kapa Biosystems, Wilmington, MA, USA) and NEBNext® Multiplex Oligos for Illumina® (Index Primers Set 1) (E7335L, NEB, Ipswich, MA, USA). Sequencing was carried out using the Illumina Xten platform as paired-end 150-bp reads.

2.15 | Single-cell RNA-seq data processing

Raw reads were demultiplexed based on cell-specific barcodes in Read2. The template switch oligo (TSO) sequence, adaptor, polyA tail, and the low-quality reads (N > 10%) were trimmed for paired Read1 using a trimmomatic (v0.36). Clean data were aligned to the mouse reference genome (mm16) using HISAT2 (v2.1.0). Gene quantification was calculated using the HTseq-count (v0.11.2).

Cells were filtered when the number of expressed genes was fewer than 200 or the mitochondrial content was greater than 15%. The Seurat (v3.1.2) pipeline was used to perform dimensionality reduction and unsupervised clustering. We used the FindAllMarkers function in Seurat to identify marker genes in each cluster. Metascape (<https://metascape.org/gp/index.html#/main/step1>) was used to perform gene ontology enrichment analysis. For assessing the cellular composition in each cluster in PDGF samples compared to vector samples, ratios of observed to expected cell numbers (Ro/e) were calculated using the Chi-square test. R function hclust and cor were used to perform the unsupervised hierarchical clustering and gene expression correlation analysis.

2.16 | Single-cell RNA-seq data analysis

Raw sequencing data were trimmed to remove adapter and low-quality reads using trimmomatic (v0.36). Quality control of sequencing data was performed by using Fast QC. Clean data were aligned to the mouse reference genome (mm16) using HISAT2 (v2.1.0). After reads mapping, the gene expression level was calculated with unique molecular identified (UMI) information by the HTseq-count. Cells with less than 200 genes were removed for further analysis. After removing ribosomal proteins and mitochondrial genes, Find Variable Genes were used in Seurat to select variable genes. Dimensionality reduction was performed using those variable gene expression data. The principal component analysis (PCA) was performed and the first 20 principal components were selected. Pericytes were clustered using Find Neighbors and Find Clusters in Seurat and visualized with uniform manifold approximation and projection (UMAP). To integrate pericyte dataset and erythroid cell datasets, we used the Integrate Data to remove batch effect and visualized with UMAP. For differential gene expression, we used the Find Markers in Seurat to find differentially expressed genes between cluster 4, 5, 7 in T241-vector group and aggregated erythroid cells. After filtering genes ($\text{lavg_logFC} \geq \log(2)$, $\text{pct.1} \geq 0.1$ or $\text{pct.2} \geq 0.1$, $\text{p_val_adj} \leq 0.05$), gene ontology enrichment analysis was performed using Cluster Profiler (v4.6.0).

2.17 | Gene set enrichment analysis (GSEA) of cell type-specific gene sets

Cell marker gene sets utilizing single-cell sequencing data in mouse were obtained from CellMarker (<http://biocc.hrbmu.edu.cn/CellMarker/download.jsp>) [57]. Single-sample GSEA (ssGSEA) was adopted to calculate the enrichment scores of different cell-type signatures,

which represented the activity level of the biological process in individual cell-type [58, 59]. Gene expression data acquired from pericytes upon the stimulation of PDGF-B (Gene Expression Omnibus (GEO) database (GSE85955)) were employed to ssGSEA, and similarity of cell-type signatures was analyzed. Enrichment scores with a P value < 0.05 in individual cell types were presented.

2.18 | Isolation of pericytes and sampling collection for microarray

Pericytes were collected from the lung and cultured. Briefly, C57/BL6 mice were euthanized using CO_2 , and the lungs were removed. The lungs were cut into small pieces and digested in a 0.15% collagenase II solution in DMEM for 1 h at 37°C . The single-cell suspension was prepared in Roswell park memorial institute (RPMI)-1640 medium (R8758, Merck), and RBCs were lysed using ammonium chloride (BD Pharmingen). After a blocking step in PBS containing 0.1% bovine serum albumin, cells were incubated with a rabbit anti-mouse NG2 antibody (1: 50, AB5320, Merck) for 1 h on ice, followed by a goat anti-rabbit Cy3 antibody (1: 200, AP187C, Millipore). Stained cells were resuspended in PBS containing 0.1% goat serum, and NG2^+ cells were sorted with the FACS Vantage/Divi (Becton Dickinson, Franklin Lakes, NJ, USA). Isolated cells were cultured in endothelial cell growth medium-2 (EGM-2, CC-3162, Lonza, Basel, Switzerland), containing 10% fetal calf serum (FCS; N4637, Merck) for 1-3 passages and cultured further in DMEM with 10% FBS for experiments. For RNA sample collection for microarray analysis, NG2^+ cells were incubated with DMEM containing 2% FBS at 37°C overnight, followed by the addition of PDGF-B in the medium. Three biological replicates for each condition (unstimulated samples as a control) were set, and RNAs were isolated utilizing RNAeasy kit (74004, Qiagen). Affymetrix 1.0 ST Gene arrays (Santa Clara, CA, USA) were employed, and data have been deposited in the GEO (accession number GSE85955).

2.19 | Microarray data analysis

Robust Multi-array Average (RMA)-normalized gene expression data of PC and S17 stromal cells treated with and without PDGF-B were downloaded from the GEO database (GSE85955 [34] and GSE33717 [23]). Differential expression analysis between PDGF-B-treated (5 days in PC and 72 h in S17) and control was performed using the R (v 4.0.3) package RankProd (v 3.16.0) [60]. Gene ontology (GO) annotations of mouse genes were obtained from http://ge-lab.org/gskb/2-MousePath/MousePath_GO_gmt.gmt.

GSEA was performed with GSEA (v4.1.0) using the GSEAPreranked tool [58], where genes were preranked based on their log fold changes. Upregulated genes with false discovery rate (FDR) < 0.05 were subjected to the UniProt tissue expression (UP_TISSUE) analysis tool in DAVID (<http://david.abcc.ncifcrf.gov/>). Radar plot analyses were performed using CellRadar (<https://github.com/KarlssonG/cellradar>). The predetermined cell type-specific gene sets were minimum-maximum scaled along with the median value across cell types.

2.20 | Database analysis

The head and neck squamous cell carcinoma (HNSC) and the pheochromocytoma and paraganglioma (PCPG) transcriptome profiling datasets (HNSC; $n = 504$, PCPG; $n = 184$) from TCGA were downloaded from the GDC Data Portal website (<https://portal.gdc.cancer.gov/>). Statistical analyses and visualization were performed using R version 4.2.1. Spearman's correlation analysis was performed between the gene expression (transcripts per kilobase million, TPM) of the genes (*PDGFB* and *CD71*; *PDGFB* and *EPO*).

2.21 | Statistics

Statistical analyses for enrichment analysis of cell type-specific gene sets, microarray data analysis, and single-cell RNA-seq were stated in each method description. Statistical analyses of other results were performed using the standard two-tailed Student *t*-test, and $P < 0.05$ was considered statistically significant. Data were presented as means \pm standard error of measurement.

3 | RESULTS

3.1 | PDGF-B drives pericyte differentiation towards the erythroblast lineage

To study the stemness features of perivascular cells, we isolated primary NG2⁺ pericytes from the mouse lung tissue. It is known that NG2⁺ pericytes express PDGFRs and respond to PDGF-B, a multipotent form in the PDGF family, which activates both PDGFR α and PDGFR β [27, 28, 61]. The primary NG2⁺ pericytes were stimulated with PDGF-B, and mRNAs were subjected to the whole genome expression profiling (Figure 1A). To define the identity of the PDGF-B-stimulated NG2⁺ pericytes, the

whole genome expression profiles were blasted against the known database of various cell types. Interestingly, the PDGF-B-stimulated NG2⁺ pericytes possessed stem cell or progenitor cell features, including neuronal stem cells, stem cells of the epithelial basal layer, mesenchymal progenitor cells, embryonic endocardial cells, fibroblasts, and BM erythroid cells, etc. (Supplementary Figure S1A).

On the basis of these findings, we pursued our interests by focusing on a possible link between NG2⁺ pericytes and HSPCs. Detailed analysis of the PDGF-B-stimulated NG2⁺ pericytes revealed the similarity of their progeny to the BM-erythroid cells (Figure 1B). This result was further validated by independent analysis employing radar plot analysis, indicating that the PDGF-B-stimulated NG2⁺ pericytes enriched in cell types in the erythroid lineage (Figure 1C). To further define the identity of these cells, we applied the hematopoiesis-related gene dataset for detailed analysis. Noticeably, the PDGF-B-stimulated NG2⁺ pericytes resembled hematopoietic progenitor cells (HPCs; Figure 1D).

Since stromal fibroblasts also express PDGFRs and respond to PDGF-B stimulation [33, 62], we employed BM-derived stromal fibroblasts S17 as controls to determine the plausible restriction of hematopoietic progenitor to NG2⁺ pericytes. GO analysis discovered that the PDGF-B-stimulated NG2⁺ pericytes were enriched with hematopoiesis-related genes, while BM-derived stromal fibroblasts represented opposing responses with those genes (Figure 1E-F). Along with this notion, the PDGF-B-stimulated NG2⁺ pericytes also shared the highest resemblance with BM (Figure 1G). By contrast, the PDGF-B-stimulated BM-derived stromal fibroblasts lacked hematopoietic features (Figure 1E-G). These results show that PDGF-B drives the differentiation of NG2⁺ pericytes towards the hematopoietic lineage.

3.2 | PDGF-B induces EPO production in the tumor stroma

We previously reported that tumor-derived PDGF-B instigated splenomegaly and hepatomegaly in tumor-bearing mice by inducing EPO expression in stromal fibroblasts [23]. To study if PDGF-B was able to induce EPO production in CAFs, we employed syngeneic tumor mouse models using PDGF-B-overexpressing Lewis lung cancer (LLC) and fibrosarcoma (T241) cells. Quantitative analysis of *Epo* mRNA levels by qPCR in tumor tissues demonstrated an approximately 7-fold increase of EPO production in PDGF-B-LLC tumors relative to vector tumors (Figure 1H). These findings were validated by an independent mouse fibrosarcoma model (Figure 1H). Consistent with increases of *Epo* mRNA levels, EPO protein levels in PDGF-B-tumor

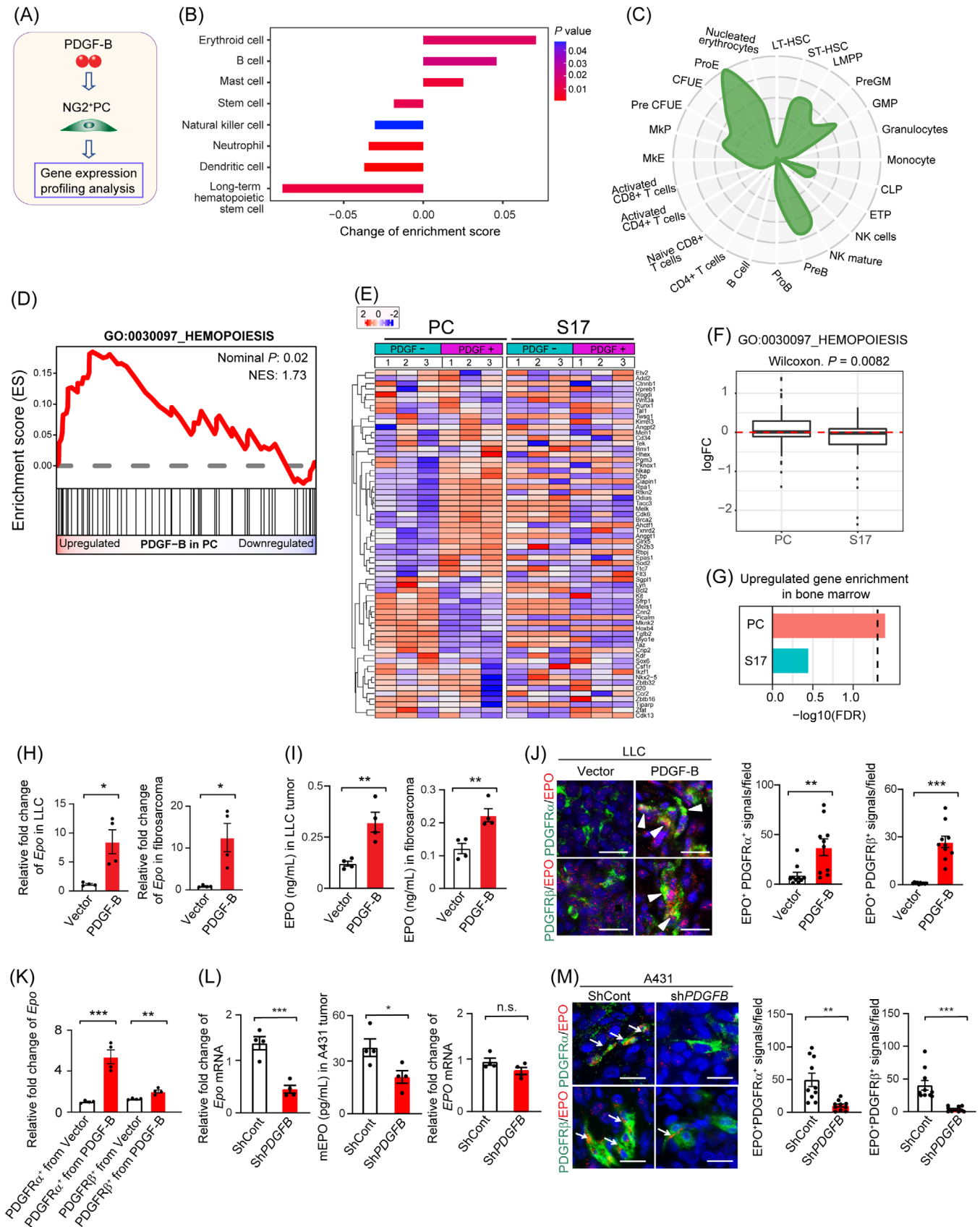


FIGURE 1 Gene-expression profiling and elevated expression levels of EPO in stromal cells, (A) Schematic diagram shows the experimental design for gene expression analysis of the PDGF-B-stimulated NG2⁺ PCs. (B-G) Microarray data obtained from PCs were analyzed by comparing various gene sets. (B) Enrichment score analysis of PDGF-B-stimulated NG2⁺ PCs against cell type-specific gene sets in the BM. Cell types with significant scores in the top 8 were presented. (C) Radar plot analysis of PDGF-B-stimulated NG2⁺ PCs within the

tissues were accordingly increased (Figure 1I). These findings show that PDGF-B induces EPO production in tumor tissues.

We next investigated the cell types that were responsible for EPO production. Interestingly, EPO protein expression was colocalized with PDGFR α and PDGFR β positive signals, which were expressed on the surface of CAFs (Figure 1J). To further validate these findings, we isolated the PDGFR $^+$ cells, CD31 $^+$ endothelial cells, NG2 $^+$ pericytes, F4/80 $^+$ macrophages from tumors and showed that these PDGFR $^+$ cells were the primary cell source for EPO production (Figure 1K; Supplementary Figure S1B). Interestingly, LLC-vector tumor cells and LLC-PDGF-B tumor cells completely lacked *Epo* expression (Supplementary Figure S1B). Again, the high EPO production was restricted to PDGF-B $^+$ tumors, but not to vector tumors. We further confirmed these findings using a human cancer cell line, A431, which is known to produce a high level of endogenous PDGF-B [33, 63]. Indeed, in A431 tumors, mouse *Epo* mRNA and protein levels were significantly elevated compared to sh*PDGFB*-A431 tumors, while tumor-derived human EPO levels were not altered by sh*PDGFB* (Figure 1L). Mouse *Epo* co-expression with PDGFR α^+ and PDGFR β^+ cells was detected in A431 tumor tissues (Figure 1M). These findings are compelling evidence for the human relevance of our findings.

3.3 | Genetic tracing of NG2 $^+$ cells in tumor tissues

In order to trace the fate of pericyte differentiation in tumors, we generated a genetic strain of mice that

carry *NG2-CreERT2:R26R-tdTomato* in pericytes. This strain of mice has successfully been used to trace pericytes in tumor tissues by accompanying tdTomato fluorochrome [33]. To generalize our results but not limit them to only lung tumors, we chose a fibrosarcoma cell line. In a fibrosarcoma, the tdTomato-red signals completely overlapped with immunohistochemical staining of NG2 $^+$ signals (Supplementary Figure S2A), validating the reliability and accuracy of the genetic labeling of *NG2-CreERT2:R26R-tdTomato* pericytes. In contrast to vector tumor tissues, PDGF-B $^+$ tumors lost NG2 positive signals, but retained tdTomato-red signals (Supplementary Figure S2A). These findings suggest that PDGF-B drives differentiation of the NG2 $^+$ cells into the NG2 $^-$ cell population. Along with this notion, our recently published work demonstrated the high plasticity of NG2 $^+$ cells in the TME [33, 34]. Morphologically, the tdTomato-red-labeled cells in PDGF-B tumors resembled a fibroblast-like phenotype, which was distinctive from the NG2 $^+$ cells in vector tumors (Supplementary Figure S2A).

Since pericytes possess stemness features, we employed several stem and progenitor cell markers to further define the identity of the tdTomato-red-labeled cells in tumors. Interestingly, significant populations of tdTomato-red-labeled cells expressed Sca1, c-Kit, and CD34 stem cell markers (Supplementary Figure S2B-D). Expression levels of these stem and progenitor cell markers were significantly increased in PDGF-B tumors relative to vector tumors (Supplementary Figure S2B-D). These data indicate that tdTomato-red-labeled pericytes possess stem and progenitor cell features.

predicted hematopoiesis cell types. The predetermined cell type-specific gene sets were minimum-maximum scaled along with the median value across cell types. (D) Hemopoiesis-related genes (GO:0030097) were significantly enriched in the PDGF-B-upregulated genes in PC. (E) Heatmap of hemopoiesis-related gene expressions in PDGF-B-stimulated PCs and S17 fibroblasts. (F) Log-fold expression changes (logFC) of hemopoiesis-related genes in PDGF-B-stimulated PCs and S17. The horizontal red dashed line defines logFC = 0. (G) Enrichment of BM-related gene expression profiling of PDGF-B-stimulated PCs and S17 fibroblasts. The vertical dashed line indicates $P = 0.05$. (H) qPCR analysis of *Epo* mRNA levels in LLC tumor and fibrosarcoma tissues ($n = 4$ samples per group). (I) ELISA analysis of EPO protein levels in LLC tumor and fibrosarcoma tissues ($n = 4$ per group). (J) Representative images of tumor tissues stained with antibodies against PDGFR α (green), PDGFR β (green), and EPO (red). 4',6-diamidino-2-phenylindole (DAPI) was used for counterstaining cell nuclei. Bar = 20 μm . Quantification of EPO $^+$ /PDGFR α^+ and of EPO $^+$ /PDGFR β^+ double-positive signals in LLC tumor tissues ($n = 10$ random fields per group). (K) qPCR analysis of *Epo* mRNA levels of isolated primary PDGFR α^+ and PDGFR β^+ populations from tumor tissues ($n = 4$ samples per group). * $P < 0.05$, ** $P < 0.01$, and *** $P < 0.001$, n.s., not significant. All dot data are presented as mean \pm SEM. (L) qPCR analysis of *Epo* and *EPO* mRNA levels and mouse EPO protein levels in shCont and sh*PDGFB* A431 tumors ($n = 4$ samples per group). (M) Representative images of A431 tumor tissues stained with antibodies against PDGFR α (green), PDGFR β (green), and EPO (red). DAPI was used for counterstaining cell nuclei. Bar = 20 μm . Quantification of EPO $^+$ /PDGFR α^+ and of EPO $^+$ /PDGFR β^+ double-positive signals in A431 tumor tissues ($n = 10$ random fields per group).

Abbreviations: PDGF-B, platelet-derived growth factor B; NG2, Neural/glial antigen 2; PC, pericyte; ProE, proerythroblast; CFUE, colony forming unit-erythroid; Pre CFUE, preColony forming unit-erythroid; MkP, megakaryocyte progenitors; MKE, megakaryocyte/erythroid; LT-HSC, long term hematopoietic stem cells; ST-HSC, short term hematopoietic stem cells; LMPP, GMP, granulocyte-macrophage progenitors; CLP, common lymphoid progenitors; ETP, early T-cell precursor; NK, natural killer; EPO, erythropoietin; LLC, Luis lang carcinoma; PDGFR, platelet-derived growth factor receptor; BM, bone marrow; DAPI, 4',6-diamidino-2-phenylindole.

3.4 | Genetic tdTomato⁺ pericytes express erythroid markers

Because tdTomato⁺ pericytes retained stem and progenitor cell features and PDGF-B induced EPO expression, we next explored the possibility that PDGF-B drove pericyte differentiation towards the erythroid lineage. For this purpose, a pan-erythrocyte marker Ter119 [64] was used to stain tumor tissues. Intriguingly, in the PDGF-B⁺ tumors, a small population of tdTomato⁺ cells expressed the erythroid marker Ter119 (Figure 2A). Although the tdTomato⁺/Ter119⁺ double-positive cells represented a minor population in the tdTomato⁺ cells, these findings suggested that pericytes had the capacity for differentiation into erythrocytes. Also, the pericyte-erythrocyte differentiation was restricted to the PDGF-B⁺ tumors because no tdTomato/Ter119 double-positive cells were detectable in vector tumors by staining (Figure 2A). These results reconciled with the fact that PDGF-B stimulated EPO production in the TME. To corroborate these findings, we used another erythroid lineage marker, transferrin receptor (CD71) [65], to co-stain tdTomato⁺ cells. Similar to Ter119⁺ staining, a small fraction of CD71⁺ signals were colocalized with tdTomato⁺ cells in PDGF-B tumors (Figure 2B).

To quantify the tdTomato⁺/Ter119⁺ and tdTomato⁺/CD71⁺ cell populations, FACS analysis was performed in PDGF-B⁺ tumors and vector tumors. The tdTomato⁺/Ter119⁺ cell population represented 5.6% of the total tdTomato⁺ population in vector tumors, whereas 17.2% of tdTomato⁺/Ter119⁺ cells existed in PDGF-B⁺ tumors (Figure 2C-D; Supplementary Figure S3A-B). The tdTomato⁺/CD71⁺ cell population consisted of 24.7% of the total cell population in PDGF-B⁺ tumors and 16.1% in vector tumors (Figure 2C-D; Supplementary Figure S3A-B). To rule out the possibility of contamination from erythroid cells, we performed an experiment to lyse RBCs prior to FACS analysis. After RBC lysis, we were still able to detect Ter119⁺ cell populations (Figure 2E-F; Supplementary Figure S3C), which express similar intensity in the tdTomato⁻ population and positive controls including peripheral blood and BM samples. In PDGF-B⁺ tumors, the c-Kit⁺/Sca1⁻ HPC population markedly increased relative to those in vector tumors (Figure 2G-H; Supplementary Figure S3C). To exclude the BM-derived hematopoietic cell contamination, CD45 signals were examined in HSPC and HPC settings. Indeed, CD45⁻ HPC population significantly increased (Figure 2I-J; Supplementary Figure S3C-D), which was corresponding to the fact that the majority of NG2⁺ pericytes were CD45⁻ cells (Supplementary Figure S3E-F). These findings provide mechanistic insights into the PDGF-B-driven pericyte differentiation towards erythroid cells.

3.5 | Transcriptome analysis defines a subpopulation of pericytes closely related to megakaryocyte-erythroid progenitors

To further dissect the transcriptome heterogeneity of pericytes, we performed single-cell RNA-seq of 513 pericytes derived from PDGF and vector mouse models. The primary L⁻S⁺NG2⁺ pericytes were isolated by FACS (Figure 3A; Supplementary Figure S4A-B). Dimension reduction and unsupervised clustering of gene expression profiles showed that pericytes were clustered into 5 groups (PC1-5) with unique sets of marker genes in each cluster (Figure 3B-C; Supplementary Figure S4C-D). According to GO enrichment analysis of these marker genes, cluster PC1 highly expressed genes enriched in “extracellular matrix organization” and “vasculature development”. By contrast, clusters PC2 and PC4 were associated with immune response. Marker genes in cluster PC2 were also involved in “regulation of cytokine production” and “inflammatory response”, while cluster PC4 specifically expressed genes related to “T cell activation” and “adaptive immune response”. However, cluster PC3 specifically expressed genes were enriched in “RNA splicing” and “nucleoside monophosphate metabolic process” (Figure 3C). We also show the top ten genes in each cluster (Supplementary Figure S4E).

We next performed Chi-square test to assess cellular compositions in each cell cluster in PDGF samples compared to vector samples. We found that cluster PC1 and PC3 increased in PDGF samples, while cluster PC4 and PC5 declined (Figure 3D). We interrogated the erythroid bias with megakaryocyte-erythroid progenitors (MEPs) in each pericyte subpopulation due to further pursuits. Both unsupervised hierarchical clustering and gene expression correlation analysis showed that the PC3 cluster of pericytes was transcriptionally close to MEP (Figure 3E-G). Indeed, we found cluster PC3 highly expressed genes, for instance, *Casp3*, *Asns*, *Lyar*, and *Glo1*, that were specifically expressed in MEP [66] (Figure 3G). Together, these results indicate that PDGF-B-stimulated NG2⁺ cells are transcriptionally heterogeneous with a subpopulation that potentially prefers erythroid lineage bias.

3.6 | Formation of erythroid-like colonies by NG2⁺ pericytes

To investigate the capacity of pericytes for differentiation into erythrocytes, L⁻S⁺NG2⁺ pericytes were isolated from tumors and cultured for colony formation (Figure 4A; Supplementary Figure S4A). A methylcellulose-based M3434 medium designed for myeloid and erythroid colony formation was employed for colony assay. Freshly isolated

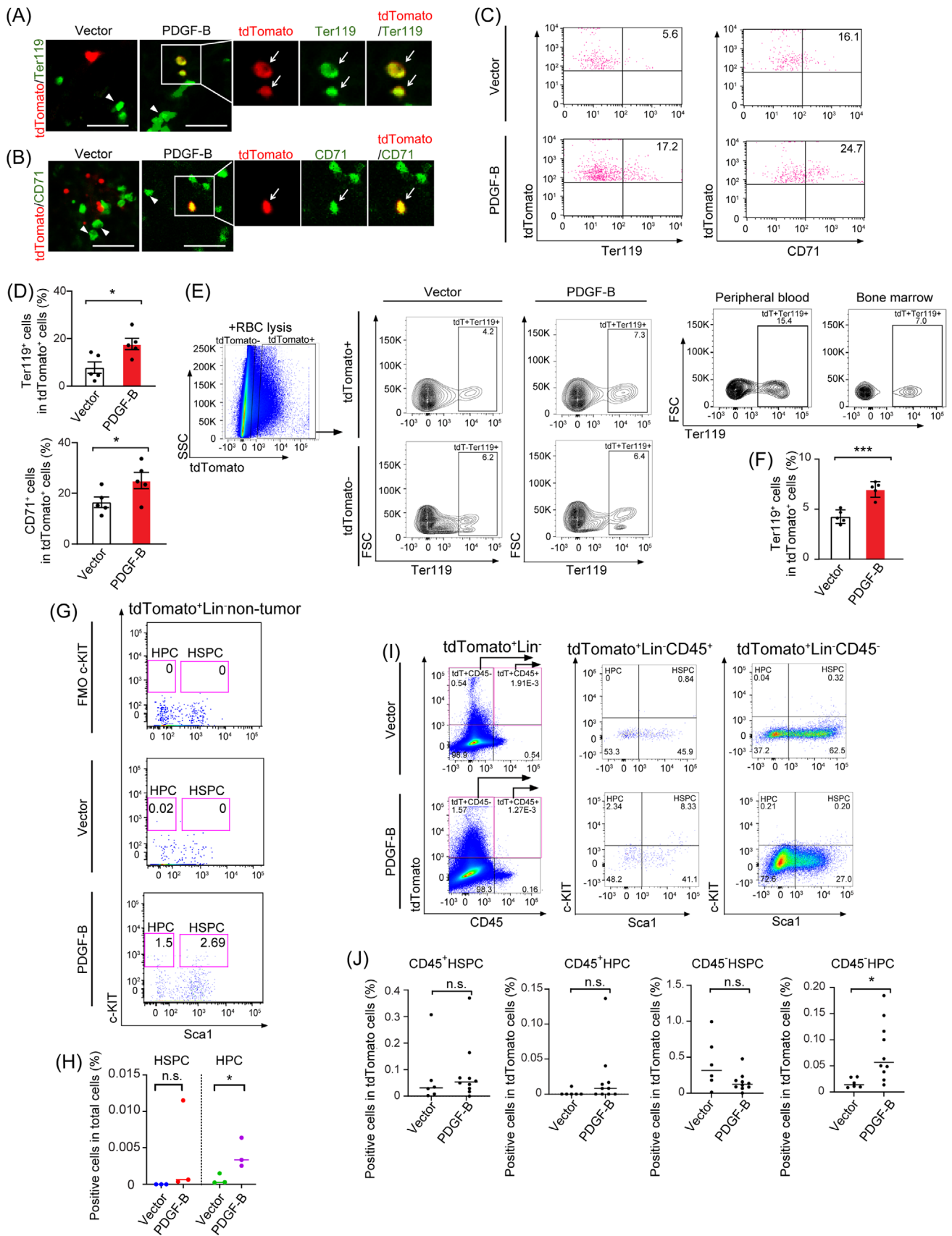


FIGURE 2 PDGF-B drives pericyte differentiation towards the erythroid lineage, (A) Representative images of tdTomato⁺ and Ter119⁺ signals in vector and PDGF-B tumors. Arrows indicate overlapping positive signals in tumor tissues. Arrowheads indicate Ter119⁺ erythroid cells. Bar = 50 μ m. (B) Representative images of tdTomato⁺ and CD71⁺ signals in vector and PDGF-B tumors. Arrows indicate overlapping positive signals in tumor tissues. Arrowheads indicate CD71⁺ erythroid cells. Bar = 50 μ m. (C) Representative FACS dot plots of

BM cells were used as a positive control. Expectedly, BM cells formed erythroid colonies, i.e., burst-forming unit-erythroid (BFU-E) (Figure 4B). Interestingly, L⁻S⁺NG2⁺ pericytes isolated from vector and PDGF-B tumors also formed erythroid-like colonies (Figure 4B), which were morphologically slightly different from BM-BFU-E. Although L⁻S⁺NG2⁺ pericytes isolated from both vector and PDGF-B tumors could form erythroid-like colonies, the L⁻S⁺NG2⁺ pericytes from PDGF-B tumors exhibited a 15-fold higher capacity relative to vector tumor pericytes to form these colonies (Figure 4C). To further validate these findings, a suspension culture system was employed for further analysis. Again, PDGF-B-L⁻S⁺NG2⁺ pericytes, but not vector-L⁻S⁺NG2⁺ pericytes, formed erythroid-like colonies (Figure 4D-E).

Consistent with erythroid morphology, L⁻S⁺NG2⁺ pericyte-derived colonies also showed positive signals of hemoglobin by benzidine staining (Figure 4F). Similarly, DAF staining validated the existence of hemoglobin in erythroid-like colonies differentiated from NG2⁺ pericytes (Figure 4G). Corresponding to these data, Giemsa staining revealed erythroblast-like morphologies in L⁻S⁺NG2⁺ pericyte-derived colonies (Figure 4H). In concordance with these data, FACS analysis demonstrated markedly increased expression of Ter119 signals with lacking CD45 signals in a majority of PDGF-B-L⁻S⁺NG2⁺ pericyte-differentiated erythroid-like colonies (Figure 4I-J; Supplementary Figure S5A). By contrast, BM LSK-derived cells differentiate into CD45⁺ cells under the same differentiation condition (Figure 4I). These results demonstrated that NG2⁺ cells from tumors differentiated into erythroid-like cells that were totally different from BM-derived hematopoietic cells. Further analysis of a panel of erythroid-specific markers, including various subunits of hemoglobin, showed increased expression in PDGF-B-L⁻S⁺NG2⁺ pericytes relative to vector-pericytes (Figure 4K). It should be emphasized that the

expression levels of these genetic markers were relatively lower than those in BM cells. Along differentiation, pericyte markers, including *Pdgfra*, *Pdgfrb*, and *Cspg4* (*Ng2*) were downregulated (Figure 4L).

3.7 | Gain- and loss-of-function PDGF and EPO in erythroid-like colony formation

To decipher molecular mechanisms underlying erythroid-like colony formation, gain- and loss-of-function approaches were employed in our experimental settings (Figure 5A). PDGF-B-tumor-bearing mice were treated with specific neutralizing antibodies against PDGFR α and PDGFR β (PDGFR blockades) [63, 67, 68]. Expectedly, after treatment with PDGFR β blockade, the isolated NG2⁺ pericytes significantly lost their ability to form the erythroid-like colonies (Figure 5B). By contrast, the PDGFR α blockade had little effect on colony formation (Figure 5B). Reconciling with these *in vivo* findings, *in vitro* treatment of NG2⁺ pericytes isolated from PDGF-B tumors with PDGFR β blockade largely attenuated their ability of colony formation (Figure 5C). Again, PDGFR α blockade had almost no impact on the erythroid-like colony formation (Figure 5C).

We next performed gain-of-function experiments by adding an exogenous PDGF-B recombinant protein to the pericyte differentiation assay. Noticeably, PDGF-B recombinant protein markedly increased the erythroid-like colony formation (Figure 5D). Similarly, PDGF-D, another PDGFR β -binding ligand [69], also significantly increased the colony numbers (Figure 5D). Conversely, PDGF-A, a PDGFR α -specific ligand [70], lacked the ability to augment colony formation in this experimental setting (Figure 5D). These findings suggest that PDGFR β is the key receptor for stimulation of erythroid-like colony formation. Along with this view, PDGFR β blockade, but

tdTomato⁺/Ter119⁺ and tdTomato⁺/CD71⁺ signals in vector and PDGF-B tumors. (D) Quantification of tdTomato⁺/Ter119⁺ signals and tdTomato⁺/CD71⁺ signals in proportion to the total tdTomato⁺ cells in vector and PDGF-B tumors ($n = 5$ biological samples per group). Data are presented as mean \pm SEM. (E) Representative FACS dot plots of tdTomato⁺ Ter119⁺ signals in vector and PDGF-B tumors. RBCs were removed by RBC lysis buffer prior to staining. Samples from peripheral blood and BM were used as positive controls. (F) Quantification of tdTomato⁺Ter119⁺ signals in proportion to the total tdTomato⁺ cells in vector and PDGF-B tumors ($n = 5$ biological samples per group). Data are presented as mean \pm SEM. (G) Representative FACS profiles showing sorting of tdTomato⁺ Lin⁻ c-Kit⁺ Sca1⁻ HPCs and tdTomato⁺ Lin⁻ c-Kit⁺ Sca1⁺ stem and progenitor cells (LSK-HSPC). After mononuclear cells were gated from 7AAD⁻ live cells, excluding the GFP⁺ tumor cells, and hematopoietic lineage (Lin), and tdTomato⁺, the remaining cells were further subfractionated by plotting Sca1 vs. c-Kit (CD117). The Lin⁻ Sca1⁺ c-Kit⁺ HSPCs and the further differentiated progenitor Lin⁻ Sca1⁻ c-Kit⁺ HPCs were gated according to FMO control. (H) Quantification of FACS analysis of HPC and HSPC populations in vector or PDGF-B tumors ($n = 3$ biological samples per group). (I) Representative FACS profiles showing sorting of tdTomato⁺ CD45⁻ Lin⁻ c-Kit⁺ Sca1⁻ HPC, tdTomato⁺ CD45⁻ Lin⁻ c-Kit⁺ Sca1⁺ HSPC, tdTomato⁺ CD45⁻ Lin⁻ c-Kit⁺ Sca1⁻ HPC, tdTomato⁺ CD45⁻ Lin⁻ c-Kit⁺ Sca1⁺ HSPC in vector and PDGF-B tumors. (J) Quantification of FACS analysis of CD45⁺ HPC, CD45⁺ HSPC, CD45⁻ HPC, and CD45⁻ HSPC populations in vector or PDGF-B tumors ($n = 6-10$ biological samples per group). * $P < 0.05$, ** $P < 0.01$, *** $P < 0.001$, n.s., not significant. Data are presented as individual values and mean determinants. Abbreviations: PDGF-B, platelet-derived growth factor B; RBC, red blood cell; FACS, Fluorescence activated cell sorting; HSPC, hematopoietic stem and progenitor cell; HPC, hematopoietic progenitor cell; BM, bone marrow; FMO, fluorescence minus one.

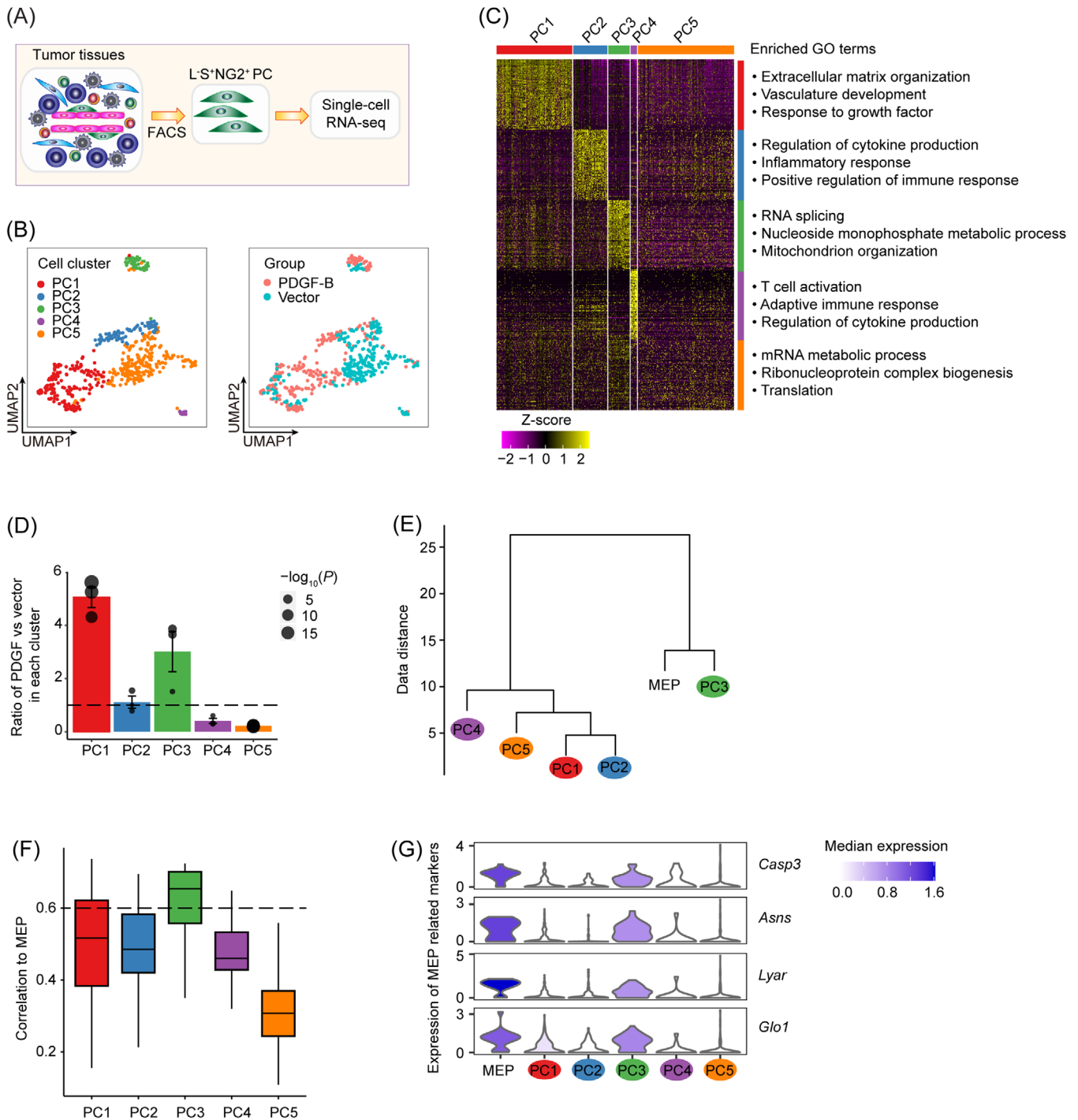


FIGURE 3 Classification of pericyte subpopulations and association to hematopoietic progenitors by single-cell RNA sequencing, (A) An experimental scheme for isolating L⁻S⁺NG2⁺ PCs for single-cell RNA-seq analysis, (B) UMAP visualization of pericytes colored by cell clusters (left panel) and sample groups (right panel), (C) Heatmap indicates cluster marker genes (top 100 genes for each cluster). The top three enriched GO terms (ranked by adjusted P-values, Benjamini-Hochberg correction) of marker genes in each cluster are shown on the right, (D) Bar plots show the ratio of observed to expected cell numbers of each cluster in PDGF samples compared to vector samples. Dots indicate three PDGF replicates and sizes represent $-\log_{10}(P)$ (Chi-square test). Error bars represent mean \pm standard errors. The dashed line indicates the threshold of vector samples, (E) Hierarchical clustering (a complete linkage method) demonstrates transcriptional similarities between MEP and pericyte clusters, (F) Box plots show the spearman correlation between MEP and single cells in each pericyte cluster, (G) Violin plots represent expressions of four MEP-specific genes in MEP and each pericyte cluster. Colors represent median expression in each cluster

Abbreviations: NG2, Neural/glial antigen 2, L⁻S⁺NG2⁺ PC, Lineage⁻ SCA1⁺ NG2⁺ pericyte; PC, pericyte; PDGF, platelet-derived growth factor; UMAP, Uniform Manifold Approximation and Projection; GO, gene ontology; MEP, megakaryocyte-erythroid progenitor; RNA, Ribonucleic acid.

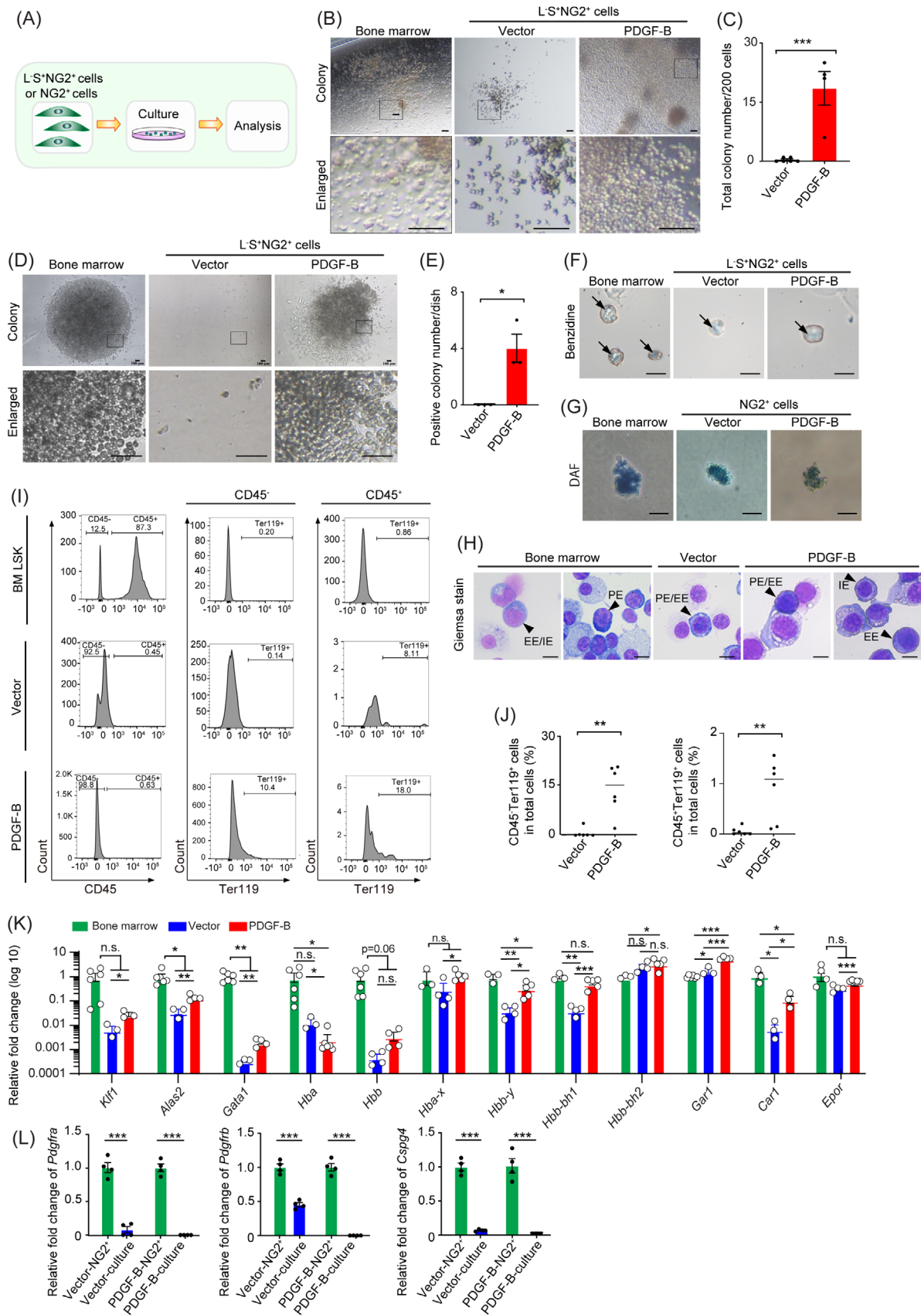


FIGURE 4 Colony formation of pericyte-derived hematopoietic progenitors in vitro, (A) The schematic diagram shows the colony formation design. Isolated primary L^S+NG2⁺ or NG2⁺ cells from tumors were cultured for hematopoietic lineage differentiation, (B) Representative pictures of the burst-forming unit-erythroid (BFU-E)-like colonies cultured in a complete methylcellulose-based medium (M3434). BM cells and L^S+NG2⁺ cells from vector and PDGF-B tumors were used for colony formation analysis. BFU-E colonies from BM

not PDGFR α blockade, completely abrogated the PDGF-B-induced colony formation (Figure 5E), supporting the role of PDGFR β in instigating colony formation.

Since EPO levels were markedly increased in PDGF-B tumors, we treated the PDGF-B tumor-bearing mice with an anti-EPO neutralizing antibody (EPO blockade). Interestingly, EPO blockade augmented rather than mitigated colony formation (Figure 5F-G). Because EPO was involved in the later stage of erythroid differentiation, blocking EPO-induced erythroblast maturation would increase the number of undifferentiated progenitor cell populations [71]. This might be the reason for the anti-EPO effect in enhancing colony formation. Indeed, treatment of the *NG2-CreERT2:R26R-tdTomato* tracing mice with EPO blockade significantly mitigated the number of mature Ter119⁺ erythrocytes in PDGF-B tumors (Figure 5H). Inversely, delivery of EPO recombinant protein in vivo in vector tumors reduced erythroid-like colony formation but increased the Ter119⁺ population (Figure 5I-K). Together, these data show that the PDGFR β signaling and EPO play crucial roles in regulating pericyte differentiation towards the erythroid lineage.

To relate our findings to clinical relevance, we used a human cancer originated from the A431 squamous carcinoma. As seen in mouse tumors, treatment of A431 cancer-bearing mice with PDGF blockade using the shPDGFB system largely ablated the formation of erythroid-like colonies by tumor pericytes (Figure 5L). Since A431 cancer is a naturally occurring high PDGF-B-producing human cancer, these findings ascertain the human relevance of our findings. To further validate our results in clinical settings,

we performed TCGA database analysis of patient cohorts of head and neck squamous cell carcinoma (HNSC) and pheochromocytoma and paraganglioma (PCPG). The total number of HNSC and PCPG patients included in this study was 504 and 184, respectively. Notably, the human A431 cell line we used in our preclinical models belongs to the HNSC types. Interestingly, *EPO* expression was correlated with *PDGFB* expression in both datasets (Supplementary Figure S5B). Furthermore, transferrin receptor 1 (*TFRC*, also known as CD71) was also correlated with *PDGFB* expressions in these datasets (Supplementary Figure S5C). These human-related data link our preclinical findings to clinical relevance.

3.8 | Insignificant contribution of BM cells in erythroid-like colony formation

It was possible that BM-derived cells significantly participated in erythroid-like colony formation in our in vivo experimental settings. To exclude this possibility, we analyzed the BM populations of the Lin⁻Sca1⁺c-Kit⁺NG2⁺ and L⁻S⁺NG2⁺ pericytes. Interestingly, BM completely lacked these pericyte populations (Figure 6A-B). Since BM micro-vessels consist of sinusoidal structures, these vasculatures usually lack the abundance of pericytes [72].

To further exclude the possibility of involvement of BM cells in the erythroid lineage differentiation in tumors, we performed BM transplantation experiments in which CD45.1 donor BM was transplanted into the irradiated CD45.2 recipient mice (Figure 6C; Supplementary

cells were used as controls. Lower panels show amplified pictures. Bar = 100 μ m, (C) Quantification of the total colony numbers in vector and PDGF-B tumors ($n = 4-6$ samples per group), (D) Representative images of colonies cultured in a liquid culture system. BM cells and L⁻S⁺NG2⁺ cells from vector and PDGF-B tumors were used for colony formation analysis. BFU-E colonies from BM cells were used as controls. Lower panels show amplified pictures. Bar = 100 μ m, (E) Quantification of colony numbers cultured in a liquid medium in vector and PDGF-B tumors ($n = 3$ samples per group), (F) Representative images of benzidine staining of colonies cultured in a complete M3434 methylcellulose-based medium. Benzidine-reactive colonies show blue signals. Arrows indicate benzidine-reactive signals. BM cells, L⁻S⁺NG2⁺ cells isolated from vector and PDGF-B tumors were used. Bar = 10 μ m., (G) Representative images of M3334 medium-cultured positive colonies stained with 2,7-diaminofluorene (DAF). BM cells, NG2⁺ cells isolated from vector and PDGF-B tumors were used. Bar = 20 μ m, (H) Representative images of Giemsa staining of colonies cultured in a M3434 methylcellulose-based medium. Arrowheads indicate various stages of erythroblasts. PE; Proerythroblast, EE; Early erythroblast, IE; Intermediate erythroblast. BM cells, L⁻S⁺NG2⁺ cells isolated from vector and PDGF-B tumors were used. Bar = 10 μ m, (I) Representative histograms of flow cytometry show CD45 and Ter119 signals of the L⁻S⁺NG2⁺ PC-derived colonies. Colonies formed by BM-derived LSK cells were used as a positive control, (J) Quantification of percentages of CD45⁺Ter119⁺ and CD45⁻ Ter119⁺ populations within the L⁻S⁺NG2⁺ PC-derived colonies. ($n = 6$ samples per group), (K) qPCR quantification of mRNA expression levels of a series of erythroid cell-related marker genes ($n = 3-6$ samples per group), (L) qPCR quantification of mRNA expression levels of *Pdgfra*, *Pdgfrb*, and *Cspg4* genes ($n = 4$ per group) in NG2⁺ PCs. * $P < 0.05$, ** $P < 0.01$, *** $P < 0.001$, n.s., not significant. All data are presented as mean \pm SEM.

Abbreviations: NG2, Neural/glial antigen 2; L⁻S⁺NG2⁺ cells, Lineage⁻ SCA1⁺ NG2⁺ cells; PDGF-B, platelet-derived growth factor B; BM LSK, bone marrow Lineage⁻ SCA1⁺ KIT(CD117)⁺; DAF, 2,7-Diaminofluorene; *Klf1*, krueppel-like factor 1; *Alas2*, delta-aminolevulinic synthase 2; *Gata1*, GATA Binding Protein 1; *Hba*, hemoglobin A; *Hbb*, hemoglobin B; *Hba-x*, hemoglobin X; *Hbb-y*, hemoglobin Y; *Hbb-bh1*, hemoglobin Z, beta-like embryonic chain; *Hbb-bh2*, hemoglobin beta, bh2; *Gar1*, H/ACA snoRNP pseudouridylylase subunit GAR1; *Car1*, carbonic anhydrase; *Epor*, erythropoietin receptor; *Pdgfra*, platelet-derived growth factor receptor alpha; *Pdgfrb*, platelet-derived growth factor receptor beta; *Cspg4*, chondroitin sulfate proteoglycan 4.

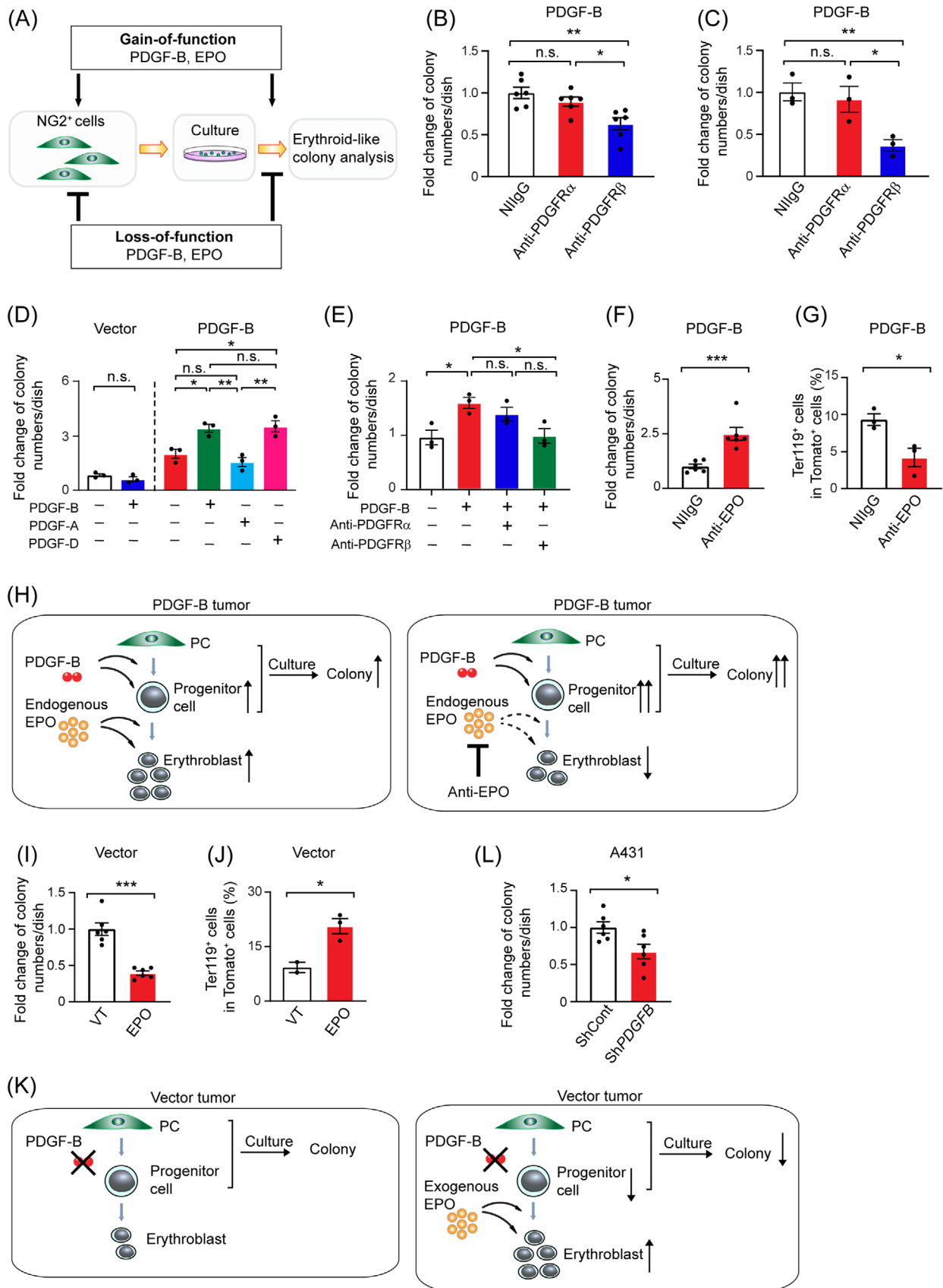


FIGURE 5 Role of PDGF and EPO signaling in pericyte-derived erythropoiesis, (A) An experimental scheme shows the gain- and loss-of-function approaches to study the impacts of PDGF and EPO in erythroid colony formation by NG2⁺ PCs, (B) Quantification of PC-derived erythroid colony numbers of in vivo-treated PDGF-B tumors by specific anti-PDGFR α and anti-PDGFR β antibodies or NiligG ($n = 6$ samples per group). Data were pooled from two independent experiments, (C) Quantification of PC-derived erythroid colony numbers in

Figure S6A-B). After 2-month transplantation, the chimeric animals showed predominantly CD45.1⁺ and a few CD45.2⁺ hematopoietic cells in peripheral blood and BM (Supplementary Figure S6C). Tumors were then implanted into the recipient animals. L⁻S⁺NG2⁺ pericyte-formed colonies were subjected to FACS analysis (Figure 6C). Convincingly, no CD45.1⁺ cells were found in the CD71⁺ population (Figure 6D-E; Supplementary Figure S6D), indicating that the CD45.1 donor BM cells did not entail in pericyte differentiation into the erythroid lineage.

4 | DISCUSSION

Using genetic tracing animal models and single-cell sequencing, we described a novel concept of erythropoiesis within solid tumor tissues. Perivascular localized NG2⁺ cells in tumor became HSPC and process erythropoiesis under the regulation of CAF-derived EPO and tumor-derived PDGF-B. Under physiological conditions, hematopoiesis is a well-defined hierarchy differentiation process from HSCs into lineage-specific progenitor cells and eventually various mature hematopoietic cells. This specialized process occurs in specialized organs, including BM, liver, and spleen, where HSCs are populated and appropriate hematopoietic microenvironments exist. Along with our discovery, recent studies also showed that the lung tissue was another potential hematopoietic organ for producing megakaryocytes and platelets [51]. To ensure hematopoiesis, several crucial elements should simultaneously coexist, including: (1) HSCs or progenitor cells that possess intrinsic potentials for differentiation; (2) Hematopoietic organ-released factors in the local microenvironment to drive differentiation of progenitors cell into various lineages; (3) Stromal cells that function as feeder

cells to facilitate hematopoiesis; (4) Endocrine hormones, such as EPO to drive erythropoiesis; and (5) Sinusoidal micro-vasculatures for disseminating hematopoietic cells into the circulation.

In this work, we showed that a solid tumor possessed all these essential prerequisites to produce its own RBCs. We demonstrated that perivascular localized cells in tumors exhibited stem and progenitor-like cell features and could differentiate into hematopoietic cells under PDGF-B stimulation. Our surprising initial findings were obtained from gene-expression profiling in PDGF-B-stimulated NG2⁺ pericytes, demonstrating that the clusters of genes resembled erythroblast features. This notion is astonishing because erythropoiesis was believed to be an organ-specific and highly regulated process only occurring in specialized organs, such as the BM and liver [41, 47]. Based on this initial observation, we hypothesized that perivascular localized cells might function as hematopoietic stem or progenitor cells. In genetic tracing experiments that permitted us to trace cell differentiation or fate changing, we found that NG2⁺ cells expressed erythroblast markers in solid tumors. PDGF-B-expressing tumor-isolated NG2⁺ cells also expressed HSC and progenitor markers and differentiated into erythrocytes *in vitro*. We should emphasize that the tumor-derived hematopoietic cells mainly belonged to noncanonical hematopoietic cells that lacked CD45 expression and retained some of the mesenchymal markers, such as NG2. Probably, these unique features are the most interesting and important parts of our discoveries. At this time of writing, it is still unclear to which discrete step of the hematopoietic differentiation tree NG2⁺ cells belong. Our feeling is that NG2⁺ cells might act as multipotent or pluripotent stem cells, which have capacities to differentiate into different lineages of hematopoietic cells. This interesting issue warrants further investigation. Although NG2⁺ cells are abundant in

the absence or presence of an anti-PDGFR α or an anti-PDGFR β antibody ($n = 3$ samples per group, 2 repeats), (D) Quantification of PC-derived erythroid colony numbers after treatment with PDGF-B, PDGF-A, and PDGF-D proteins in culture ($n = 3$ samples per group, 2 repeats), (E) Quantification of PC-derived erythroid colony numbers after treatment with PDGF-B protein in the absence or presence of an anti-PDGFR α or an anti-PDGFR β antibody ($n = 3$ samples per group, 2 repeats), (F) Quantification of PC-derived erythroid colony numbers after treatment with an anti-EPO antibody and NIIgG ($n = 6$ samples per group. Data were pooled from two independent experiments), (G) Quantification of tdTomato⁺/Ter119⁺ signals by FACS in PDGF-B tumors treated by an anti-EPO antibody and NIIgG *in vivo* ($n = 3$ samples per group), (H) Blocking endogenous EPO decreases erythroblasts, but increases the pericyte-derived erythroid progenitor pool, (I) Quantification of PC-derived erythroid colony numbers after treatment with *in vivo*-treated by EPO protein and vehicle ($n = 6$ samples per group, Data were pooled from two independent experiments), (J) Quantification of tdTomato⁺/Ter119⁺ signals by FACS in vector tumors after *in vivo* treatment with EPO protein and vehicle ($n = 3$ samples per group), (K) Vector tumors lack sufficient PDGF and EPO to expand the pericyte-derived erythroid progenitor pool and erythroblast differentiation. Exogenous EPO promotes an increase of erythroblasts, while a progenitor pool decreases due to lack of PDGF-B. NIIgG = Nonimmune IgG; VT = vehicle treatment, (L) Quantification of colony numbers in scrambled-shRNA and shPDGFB A431 tumors ($n = 6$ samples per group, Data were pooled from two independent experiments). * $P < 0.05$, ** $P < 0.01$, *** $P < 0.001$, and n.s., not significant. Data are presented as mean \pm SEM.

Abbreviations: PDGF-B, platelet-derived growth factor B; PDGF-A, platelet-derived growth factor A; PDGF-D, platelet-derived growth factor D; EPO, erythropoietin; NG2, Neural/glia antigen 2; PFGFR α , platelet-derived growth factor receptor alpha; PFGFR β , platelet-derived growth factor receptor beta; NIIgG, nonimmune IgG.

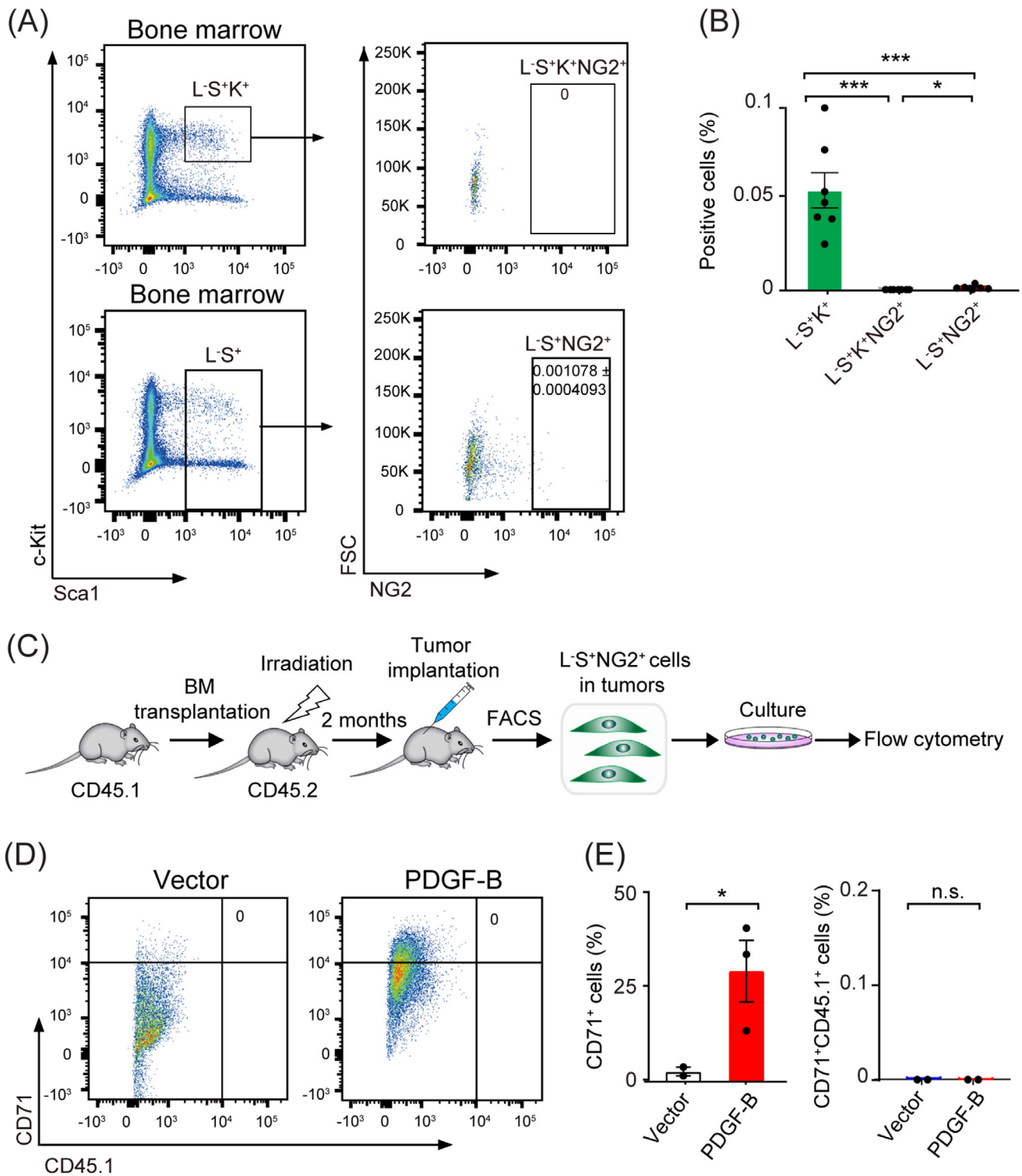


FIGURE 6 BM transplantation and tumor hematopoiesis, (A) Representative flow cytometric density plots for detecting L-S⁻K⁺, L-S⁻ and NG2⁺ populations in healthy BM, (B) Quantification of L-S⁻K⁺, L-S⁻K⁺NG2⁺, and L-S⁺NG2⁺ cell populations from BM ($n = 7$ samples per group). Percentages of positive populations in the gate, (C) The BM transplantation scheme. BM cells from CD45.1 donor mice were transplanted into the irradiated CD45.2 recipient mice. After 2-month transplantation, tumor cells were subcutaneously injected and L-S⁺NG2⁺ cells were isolated from tumors for culture analysis. Differentiated cells were further analyzed by flow cytometry, (D) Representative flow cytometric density plots for detecting CD71⁺ and CD45.1⁺ signals. Percentages of CD71⁺/CD45.1⁺ double-positive cells, (E) Quantification of CD71⁺ and CD71⁺CD45.1⁺ double-positive cell populations ($n = 2-3$ samples per group). * $P < 0.05$, ** $P < 0.01$, and *** $P < 0.001$. Data are presented as mean \pm SEM.

Abbreviations: L-S⁻K⁺, Lineage⁻ SCA1⁺ KIT(CD117)⁺; NG2, Neural/glial antigen 2; FSC, forward scatter; BM, bone marrow; PDGF-B, platelet-derived growth factor B.

healthy tissues, we did not observe these cells differentiate into hematopoietic cells. Perhaps, PDGF-B, EPO, and the distinguished characteristics in the TME is required for the NG2⁺ cell-derived hematopoiesis. Additionally, it is important to note that the cell population we investigated represented a small fraction of perivascular localized cells in the TME. Current technology is limited, and we cannot rule out all technical issues, such as complete absence of contamination during single-cell isolation. Our findings require validation in other pre-clinical models and clinical samples.

To ensure erythropoiesis, tumor cells promulgated stromal CAFs to produce high levels of EPO, a crucial hormone for RBC production. Under physiological conditions, EPO production was restricted to the kidney and liver, which maintains a production capacity of a maximal 10% of the total EPO synthesis [73]. Despite broad expression patterns of EpoR in various cell types, EPO primarily acted on BM proerythroblasts and erythroblasts for RBC production [74]. Thus, EPO acts as a truly endocrine hormone by targeting remote progenitor cells. Would kidney-derived EPO be sufficient to trigger erythropoiesis in tumors? Although this question remains unanswered, our data showed that additional EPO production was required in the TME to trigger this process. To circumvent this problem, tumors produced their own paracrine hormones, such as EPO to achieve a high level in the local TME (Supplementary Figure S7A-B). This paracrine mechanism was dependent on the cellular composition of the TEM and their interactions. Tumor cell-derived PDGFs stimulated expansion and activation of CAFs to increase the local levels of EPO and simultaneously repelled pericytes to enlarge the pool of hematopoietic cells (Supplementary Figure S7A-B). Additionally, in certain types of tumors, such as breast cancer, EPO could be produced by tumor cells per se [75]. Even though not investigated, we reasonably speculate that other factors, such as TGF β in TME might also play similar dual roles in facilitating tumor hematopoiesis. Alternatively, several factors may play synchronized functions by targeting stem cells and synthesizing necessary factors for erythropoiesis.

The other critical element for fulfilling the criteria of hematopoiesis is the structural and functional properties of micro-vessels, which exhibit unique sinusoidal structures that warrant the exchange of blood cells. Such sinusoidal vasculatures exist in hematopoietic organs, including BM, liver, and spleen. Similarly, tumor vasculatures also consisted of sinusoidal micro-vessels, which were highly leaky and exchangeable with cellular contents in the TME [76]. Additionally, tumor micro-vessels provided an abundant source of perivascular HPCs to cope with the increasing oxygen demands. Thus, tumor micro-vasculatures also match the hematopoietic criterium for

disseminating hematopoietic cells to distal organs. Apart from the intrinsic ability to produce hematopoietic cells in tumors, tumor-derived RBCs have to be transported to the lung for oxygen exchange. Admittedly, we do not know the functional significance of the tumor-derived RBCs in participating in the total oxygen exchange in promoting tumor growth. Perhaps, in some tumors, especially hypoxic tumors and in anemic cancer patients, the production of supplementary RBCs plays a determinant role in facilitating tumor growth and metastasis.

Furthermore, the biological advantage of producing its own blood cells in the TME might improve hypoxia. Tumors obtain the adaptation system against hypoxia, leading to altering their metabolism, activating a migratory ability, and remodeling the extracellular matrix to survive. However, it is more beneficial to avoid a hypoxia environment as tumors maintain their characteristics in an anabolic state and maintain proliferative activity. Other than oxygenation, these blood cells may produce cytokines and signaling molecules that are potentially beneficial for tumor growth. Moreover, the advantage of producing the RBC at the tumor site may (1) produce RBCs in a bone-marrow independent manner by tumor tissue-produced EPO; (2) increase the total RBC number without exhaustion of BM; (3) increase the production of tumor-derived RBCs throughout the tumor growth period. These interesting issues warrant future studies.

5 | CONCLUSIONS

Our findings provide a novel mechanistic paradigm in understanding PDGF-B- and EPO-regulated differentiation of NG2⁺ perivascular progenitor cells towards the erythroid lineage in the TME. Targeting tumor erythropoiesis may provide a novel therapeutic concept for treating solid cancers.

DECLARATIONS

AUTHOR CONTRIBUTIONS

Yihai Cao generated the initial idea. Yihai Cao, Kayoko Hosaka, Yunlong Yang, and Yuanfu Xu designed experiments. Kayoko Hosaka, Shiyue Zhang, and Xue Lv performed most of the experiments and analysis. Chenchen Wang, Takahiro Seki, Yin Zhang, Xu Jing, Jieyu Wu, Qiqiao Du, Xingkang He, Yulong Fan, Xuan Li, Makoto Kondo, Masahito Yoshihara, Hong Qian, Lihong Shi, and Ping Zhu significantly contributed to experimental execution and data analysis. Tao Cheng participated in a discussion, experimental design, and data analysis. Yihai Cao wrote the manuscript.

ACKNOWLEDGEMENTS

The authors would like to thank the rest of members in Yihai Cao's laboratory (Karolinska Institute, Stockholm, Sweden) for suggestions and discussions of this work.

CONFLICT OF INTEREST STATEMENT

The authors claim no conflict of interest related to this work.

FUNDING INFORMATION

Yuanfu Xu's laboratory is supported by CAMS Innovation Fund for Medical Sciences (2021-I2M-1-017), the National Natural Science Foundation of China (81970107), State Key Laboratory of Experimental Hematology Research Grant (Z22-02), and Tianjin "131" Science Fund for Creative Research Groups (2021). Yihai Cao's laboratory is supported through research grants from the Swedish Research Council (2016-02215, 2019-01502, 2020-06121, and 2021-06122), National Key R&D Program of China (2020YFC0846600), the Hong Kong Centre for Cerebrocardiovascular Health Engineering, the Swedish Cancer Foundation (200734PjF), the Swedish Children's Cancer Foundation (PR2018-0107), the Strategic Research Areas (SFO)-Stem Cell and Regenerative Medicine Foundation, the Karolinska Institute Foundation (2020-02080), the Karolinska Institute distinguished professor award, and the Karolinska Institute Foundation (2020-02588). Kayoko Hosaka is supported by the Karolinska Institute Foundation. Takahiro Seki was supported by the Scandinavia-Japan Sasakawa Foundation. Xu Jing is supported by the National Natural Science Foundation of China (81801163) and Doctor Fund of Shandong Natural Science Foundation (ZR201807060846). Masahito Yoshihara is supported by the Japan Society for the Promotion of Science (JSPS) Overseas Research Fellowships.

ETHICS APPROVAL AND CONSENT TO PARTICIPATE

All animal studies were approved by the North Stockholm Animal Ethical Committee in Sweden (6196-2019, N192-13) or the Institutional Animal Care and Use Committee at the Institute of Hematology, Chinese Academy of Medical Sciences (IHCAMS-DWLL-CIFMS2021004-1).

CONSENT FOR PUBLICATION

Not applicable.

DATA AVAILABILITY STATEMENT

The data that support the findings of this study are available from the corresponding author upon reasonable request.

ORCID

Masahito Yoshihara  <https://orcid.org/0000-0002-8915-9282>

Yunlong Yang  <https://orcid.org/0000-0003-1551-9828>

Yihai Cao  <https://orcid.org/0000-0003-1308-0065>

REFERENCES

- Hanahan D, Weinberg RA. Hallmarks of cancer: the next generation. *Cell*. 2011;144(5):646–74.
- Cully M. Tumour microenvironment: Fibroblast subtype provides niche for cancer stem cells. *Nat Rev Cancer*. 2018;18(3):136.
- De Palma M, Biziato D, Petrova TV. Microenvironmental regulation of tumour angiogenesis. *Nat Rev Cancer*. 2017;17(8):457–74.
- Chen X, Song E. The theory of tumor ecosystem. *Cancer Commun (Lond)*. 2022;42(7):587–608.
- Folkman J, Hanahan D. Switch to the angiogenic phenotype during tumorigenesis. *Princess Takamatsu Symp*. 1991;22:339–47.
- Grivennikov SI, Greten FR, Karin M. Immunity, inflammation, and cancer. *Cell*. 2010;140(6):883–99.
- Clevers H. At the crossroads of inflammation and cancer. *Cell*. 2004;118(6):671–4.
- Kalluri R. The biology and function of fibroblasts in cancer. *Nat Rev Cancer*. 2016;16(9):582–98.
- Hu D, Li Z, Zheng B, Lin X, Pan Y, Gong P, et al. Cancer-associated fibroblasts in breast cancer: Challenges and opportunities. *Cancer Commun (Lond)*. 2022;42(5):401–34.
- Joyce JA, Fearon DT. T cell exclusion, immune privilege, and the tumor microenvironment. *Science*. 2015;348(6230):74–80.
- Schreiber RD, Old LJ, Smyth MJ. Cancer immunoediting: integrating immunity's roles in cancer suppression and promotion. *Science*. 2011;331(6024):1565–70.
- Pouyssegur J, Dayan F, Mazure NM. Hypoxia signalling in cancer and approaches to enforce tumour regression. *Nature*. 2006;441(7092):437–43.
- Folkman J. Angiogenesis in cancer, vascular, rheumatoid and other disease. *Nat Med*. 1995;1(1):27–31.
- Vanharanta S, Massague J. Origins of metastatic traits. *Cancer Cell*. 2013;24(4):410–21.
- Rouhi P, Jensen LD, Cao Z, Hosaka K, Lanne T, Wahlberg E, et al. Hypoxia-induced metastasis model in embryonic zebrafish. *Nat Protoc*. 2010;5(12):1911–8.
- Tabassum DP, Polyak K. Tumorigenesis: it takes a village. *Nat Rev Cancer*. 2015;15(8):473–83.
- Byrne AT, Alferez DG, Amant F, Annibaldi D, Arribas J, Biankin AV, et al. Interrogating open issues in cancer medicine with patient-derived xenografts. *Nat Rev Cancer*. 2017;17(10):632.
- Carracedo A, Cantley LC, Pandolfi PP. Cancer metabolism: fatty acid oxidation in the limelight. *Nat Rev Cancer*. 2013;13(4):227–32.
- Cairns RA, Harris IS, Mak TW. Regulation of cancer cell metabolism. *Nat Rev Cancer*. 2011;11(2):85–95.
- Cao Y. Adipocyte and lipid metabolism in cancer drug resistance. *J Clin Invest*. 2019;129(8):3006–17.
- Shen S, Vagner S, Robert C. Persistent Cancer Cells: The Deadly Survivors. *Cell*. 2020;183(4):860–74.
- Folkman J. Tumor angiogenesis and tissue factor. *Nat Med*. 1996;2(2):167–8.

23. Xue Y, Lim S, Yang Y, Wang Z, Jensen LD, Hedlund EM, et al. PDGF-BB modulates hematopoiesis and tumor angiogenesis by inducing erythropoietin production in stromal cells. *Nat Med*. 2011;18(1):100–10.
24. Armulik A, Genove G, Betsholtz C. Pericytes: developmental, physiological, and pathological perspectives, problems, and promises. *Dev Cell*. 2011;21(2):193–215.
25. Ferrara N, Kerbel RS. Angiogenesis as a therapeutic target. *Nature*. 2005;438(7070):967–74.
26. Carmeliet P, Jain RK. Angiogenesis in cancer and other diseases. *Nature*. 2000;407(6801):249–57.
27. Heldin CH, Lennartsson J, Westermark B. Involvement of platelet-derived growth factor ligands and receptors in tumorigenesis. *J Intern Med*. 2018;283(1):16–44.
28. Ostman A, Heldin CH. PDGF receptors as targets in tumor treatment. *Adv Cancer Res*. 2007;97:247–74.
29. Sasaki M, Jung Y, North P, Eelsey J, Choate K, Toussaint MA, et al. Introduction of Mutant GNAQ into Endothelial Cells Induces a Vascular Malformation Phenotype with Therapeutic Response to Imatinib. *Cancers (Basel)*. 2022;14(2):413.
30. Raica M, Cimpean AM. Platelet-Derived Growth Factor (PDGF)/PDGF Receptors (PDGFR) Axis as Target for Antitumor and Antiangiogenic Therapy. *Pharmaceuticals (Basel)*. 2010;3(3):572–99.
31. Betsholtz C, Lindblom P, Gerhardt H. Role of pericytes in vascular morphogenesis. *EXS*. 2005(94):115–25.
32. Distler JH, Hirth A, Kurowska-Stolarska M, Gay RE, Gay S, Distler O. Angiogenic and angiostatic factors in the molecular control of angiogenesis. *Q J Nucl Med*. 2003;47(3):149–61.
33. Hosaka K, Yang Y, Seki T, Fischer C, Dubey O, Fredlund E, et al. Pericyte-fibroblast transition promotes tumor growth and metastasis. *Proc Natl Acad Sci U S A*. 2016;113(38):E5618–27.
34. Hosaka K, Yang Y, Seki T, Nakamura M, Andersson P, Rouhi P, et al. Tumour PDGF-BB expression levels determine dual effects of anti-PDGF drugs on vascular remodelling and metastasis. *Nat Commun*. 2013;4:2129.
35. Abramsson A, Lindblom P, Betsholtz C. Endothelial and nonendothelial sources of PDGF-B regulate pericyte recruitment and influence vascular pattern formation in tumors. *J Clin Invest*. 2003;112(8):1142–51.
36. Rankin EB, Wu C, Khatri R, Wilson TL, Andersen R, Araldi E, et al. The HIF signaling pathway in osteoblasts directly modulates erythropoiesis through the production of EPO. *Cell*. 2012;149(1):63–74.
37. Digicaylioglu M, Lipton SA. Erythropoietin-mediated neuroprotection involves cross-talk between Jak2 and NF-kappaB signalling cascades. *Nature*. 2001;412(6847):641–7.
38. Minamishima YA, Kaelin WG, Jr. Reactivation of hepatic EPO synthesis in mice after PHD loss. *Science*. 2010;329(5990):407.
39. Semenza GL, Koury ST, Nejfelt MK, Gearhart JD, Antonarakis SE. Cell-type-specific and hypoxia-inducible expression of the human erythropoietin gene in transgenic mice. *Proc Natl Acad Sci U S A*. 1991;88(19):8725–9.
40. Ratcliffe PJ, Jones RW, Phillips RE, Nicholls LG, Bell JI. Oxygen-dependent modulation of erythropoietin mRNA levels in isolated rat kidneys studied by RNase protection. *J Exp Med*. 1990;172(2):657–60.
41. Laurenti E, Gottgens B. From haematopoietic stem cells to complex differentiation landscapes. *Nature*. 2018;553(7689):418–26.
42. Akashi K, Traver D, Zon LI. The complex cartography of stem cell commitment. *Cell*. 2005;121(2):160–2.
43. Moore KA, Lemischka IR. Stem cells and their niches. *Science*. 2006;311(5769):1880–5.
44. Herzog EL, Chai L, Krause DS. Plasticity of marrow-derived stem cells. *Blood*. 2003;102(10):3483–93.
45. Eaves CJ. Hematopoietic stem cells: concepts, definitions, and the new reality. *Blood*. 2015;125(17):2605–13.
46. Watcham S, Kucinski I, Gottgens B. New insights into hematopoietic differentiation landscapes from single-cell RNA sequencing. *Blood*. 2019;133(13):1415–26.
47. Perrine SP, Vichinsky E, Faller DV. Hematopoietic hormones: from cloning to clinic. *Am J Pediatr Hematol Oncol*. 1989;11(3):268–75.
48. Krantz SB. Erythropoietin. *Blood*. 1991;77(3):419–34.
49. Yamamoto K, Miwa Y, Abe-Suzuki S, Abe S, Kirimura S, Onishi I, et al. Extramedullary hematopoiesis: Elucidating the function of the hematopoietic stem cell niche (Review). *Mol Med Rep*. 2016;13(1):587–91.
50. Yoder MC. Embryonic hematopoiesis in mice and humans. *Acta Paediatr Suppl*. 2002;91(438):5–8.
51. Lefrancais E, Ortiz-Munoz G, Caudrillier A, Mallavia B, Liu F, Sayah DM, et al. The lung is a site of platelet biogenesis and a reservoir for haematopoietic progenitors. *Nature*. 2017;544(7648):105–9.
52. Cao Y. Angiogenesis and vascular functions in modulation of obesity, adipose metabolism, and insulin sensitivity. *Cell Metab*. 2013;18(4):478–89.
53. Mills SJ, Cowin AJ, Kaur P. Pericytes, mesenchymal stem cells and the wound healing process. *Cells*. 2013;2(3):621–34.
54. Dellavalle A, Maroli G, Covarello D, Azzoni E, Innocenzi A, Perani L, et al. Pericytes resident in postnatal skeletal muscle differentiate into muscle fibres and generate satellite cells. *Nat Commun*. 2011;2:499.
55. Picelli S, Faridani OR, Bjorklund AK, Winberg G, Sagasser S, Sandberg R. Full-length RNA-seq from single cells using Smart-seq2. *Nat Protoc*. 2014;9(1):171–81.
56. Li L, Dong J, Yan L, Yong J, Liu X, Hu Y, et al. Single-Cell RNA-Seq Analysis Maps Development of Human Germline Cells and Gonadal Niche Interactions. *Cell Stem Cell*. 2017;20(6):858–73 e4.
57. Zhang X, Lan Y, Xu J, Quan F, Zhao E, Deng C, et al. CellMarker: a manually curated resource of cell markers in human and mouse. *Nucleic Acids Res*. 2019;47(D1):D721–D8.
58. Subramanian A, Tamayo P, Mootha VK, Mukherjee S, Ebert BL, Gillette MA, et al. Gene set enrichment analysis: a knowledge-based approach for interpreting genome-wide expression profiles. *Proc Natl Acad Sci U S A*. 2005;102(43):15545–50.
59. Barbie DA, Tamayo P, Boehm JS, Kim SY, Moody SE, Dunn IF, et al. Systematic RNA interference reveals that oncogenic KRAS-driven cancers require TBK1. *Nature*. 2009;462(7269):108–12.
60. Hong F, Breitling R, McEntee CW, Wittner BS, Nemhauser JL, Chory J. RankProd: a bioconductor package for detecting differentially expressed genes in meta-analysis. *Bioinformatics*. 2006;22(22):2825–7.
61. Cao Y. Multifarious functions of PDGFs and PDGFRs in tumor growth and metastasis. *Trends Mol Med*. 2013;19(8):460–73.
62. Hoch RV, Soriano P. Roles of PDGF in animal development. *Development*. 2003;130(20):4769–84.

63. Hosaka K, Yang Y, Seki T, Du Q, Jing X, He X, et al. Therapeutic paradigm of dual targeting VEGF and PDGF for effectively treating FGF-2 off-target tumors. *Nat Commun.* 2020;11(1):3704.
64. Liu J, Mohandas N, An X. Membrane assembly during erythropoiesis. *Curr Opin Hematol.* 2011;18(3):133–8.
65. Nakahata T, Okumura N. Cell surface antigen expression in human erythroid progenitors: erythroid and megakaryocytic markers. *Leuk Lymphoma.* 1994;13(5-6):401–9.
66. Dong F, Hao S, Zhang S, Zhu C, Cheng H, Yang Z, et al. Differentiation of transplanted haematopoietic stem cells tracked by single-cell transcriptomic analysis. *Nat Cell Biol.* 2020;22(6):630–9.
67. Hosaka K, Yang Y, Nakamura M, Andersson P, Yang X, Zhang Y, et al. Dual roles of endothelial FGF-2-FGFR1-PDGF-BB and perivascular FGF-2-FGFR2-PDGFRbeta signaling pathways in tumor vascular remodeling. *Cell Discov.* 2018;4:3.
68. Yang Y, Andersson P, Hosaka K, Zhang Y, Cao R, Iwamoto H, et al. The PDGF-BB-SOX7 axis-modulated IL-33 in pericytes and stromal cells promotes metastasis through tumour-associated macrophages. *Nat Commun.* 2016;7:11385.
69. Bergsten E, Uutela M, Li X, Pietras K, Ostman A, Heldin CH, et al. PDGF-D is a specific, protease-activated ligand for the PDGF beta-receptor. *Nat Cell Biol.* 2001;3(5):512–6.
70. Heldin CH, Westermark B. Platelet-derived growth factors: a family of isoforms that bind to two distinct receptors. *Br Med Bull.* 1989;45(2):453–64.
71. Constantinescu SN, Ghaffari S, Lodish HF. The Erythropoietin Receptor: Structure, Activation and Intracellular Signal Transduction. *Trends Endocrinol Metab.* 1999;10(1):18–23.
72. Lim S, Zhang Y, Zhang D, Chen F, Hosaka K, Feng N, et al. VEGFR2-mediated vascular dilation as a mechanism of VEGF-induced anemia and bone marrow cell mobilization. *Cell Rep.* 2014;9(2):569–80.
73. Risor LM, Fenger M, Olsen NV, Moller S. Hepatic erythropoietin response in cirrhosis. *Scand J Clin Lab Invest.* 2016;76(3):234–9.
74. Kuhrt D, Wojchowski DM. Emerging EPO and EPO receptor regulators and signal transducers. *Blood.* 2015;125(23):3536–41.
75. Zhou B, Damrauer JS, Bailey ST, Hadzic T, Jeong Y, Clark K, et al. Erythropoietin promotes breast tumorigenesis through tumor-initiating cell self-renewal. *J Clin Invest.* 2014;124(2):553–63.
76. Ribatti D, Nico B, Crivellato E, Vacca A. The structure of the vascular network of tumors. *Cancer Lett.* 2007;248(1):18–23.

SUPPORTING INFORMATION

Additional supporting information can be found online in the Supporting Information section at the end of this article.

How to cite this article: Hosaka K, Wang C, Zhang S, Lv X, Seki T, Zhang Y, et al. Perivascular localized cells commit erythropoiesis in PDGF-B-expressing solid tumors. *Cancer Communications.* 2023;43:637–660.
<https://doi.org/10.1002/cac2.12423>